Mechanical, Morphological and Thermal Characterization of Compatibilized Poly(lactic acid)/Thermoplastic Starch Blends

L. Lendvai[1,2,*], D. Brenn[2]

[1]Széchenyi István University, Department of Materials Science and Engineering
Egyetem tér 1, H-9026 Győr, Hungary
***e-mail: lendvai.laszlo@sze.hu**

[2]Budapest University of Technology and Economics, Department of Polymer Engineering
Műegyetem rkp. 3, H-1111 Budapest, Hungary

Abstract: A two-step compounding procedure was used to produce binary blends composed of poly(lactic acid) (PLA) and thermoplastic starch (TPS) with varying component ratios. Subsequently, three different chemical connectors were introduced in order to enhance the interfacial adhesion between the PLA and the TPS. Maleic anhydride, blocked isocyanate, and chain extender were used as coupling agents. Mechanical, morphological and thermal properties of PLA/TPS blends were determined. It was revealed that the initial interfacial adhesion between the components is weak. Out of the three coupling agents introduced, the chain extender proved to be the most effective, however, the improvement achieved in the mechanical properties was still marginal. According to the thermogravimetric analysis thermal stability was not significantly affected by any of the coupling agents.

Keywords: *thermoplastic starch; poly(lactic acid); compatibilization; polymer blend*

1. Introduction

In the recent decades, there has been an increasing interest in reducing the amount of the waste caused by the disposable plastic products. In order to achieve this,

considerable efforts have been devoted to replace oil-based, non-degradable plastics with natural and biodegradable polymeric materials.

Starch is considered as one of the most promising candidate due to its high availability and low price. Native starch is a semi-crystalline polymer, a polysaccharide composed of amylose and amylopectin. Starch itself does not have any thermoplastic properties [1]. However, with suitable plasticizers (water, glycerol, sorbitol, etc.) it can be brought into a gelatinized form, which is called thermoplastic starch (TPS). TPS can already be processed with common thermoplastic technologies like extrusion, injection molding [2] or solution casting [3]. Despite the lots of benefits, TPS also has its drawbacks: moisture sensitivity poor mechanical properties and significant property change with elapsed time. Also a high amount of studies dealt with the topic of compounding starch with eco-friendly polyesters, such as poly(lactic acid) (PLA) [4], polycaprolactone (PCL) [5] or poly(butylene adipate-*co*-terephthalate) [6] in order to reduce their production costs and to preserve their biodegradable characteristics.

PLA is a semi-crystalline biodegradable polyester that can be made from renewable resources [7]. Due to its outstanding strength, stiffness, biocompatibility and transparency it is widely used for medical, agricultural and packaging applications [8]. In the meanwhile, PLA has relatively high production costs, it is brittle and presents limited gas barrier properties. Blending PLA with TPS could be a good strategy to obtain a more cost-efficient biodegradable material. Some works have been devoted in the recent years to the development of PLA/TPS blends [9]. Nevertheless, PLA and TPS are thermodynamically incompatible, since the interfacial adhesion between the hydrophobic PLA and the hydrophilic TPS is rather poor.

In the recent years numerous studies investigated the possibilities of introducing different reactive coupling agents in order to enhance the interfacial adhesion between TPS and PLA. When attempting to improve the mechanical properties of PLA/TPS blends, the most common way is the use of reactive compatibilizers [4].

Several researchers added difunctional molecules with high reactivity, such as methylenediphenyl diisocyanate (MDI) [10] or hexamethylene diisocyanate (HDI) [11] in order to achieve a better adhesion between the components. Hydroxyl and carboxyl groups both in TPS and PLA molecules are expected to interact with the isocyanate groups, therefore enhancing the bond between the two polymers. Note, that both MDI and HDI are recorded as harmful substances by the EU Commission Communication 2008/C 34/01 [4]. There is also an issue related to the high reactivity of commercially available chemicals: the isocyanate groups associated with urethane crosslinkers are reactive towards many other compounds. This reactivity can lead to stability problems due to the ability of NCO groups to react with atmospheric

moisture. The recently introduced blocking technology of Lanxess enables the isocyanates to remain stable on room temperature and to be thermally re-activated. By choosing a suitable blocked isocyanate grade (with a reactivation temperature just below processing temperature) it is possible to graft it on the TPS or PLA *in situ* during a reactive melt blending, thereby making the preliminary grafting procedure unnecessary.

Anhydrides with unsaturated bonds have also been used in polymer compatibilization. For the grafting procedure one requires an organic peroxide as free-radical initiator [12]. Orozco [13] and his group functionalized PLA with maleic anhydride (MA) through reactive melt blending. They used dicumyl peroxide (DCP) as an initiator of the grafting process. According to the SEM analysis the MA enhanced the compatibility between the PLA and TPS showing a stable, homogenous interface.

Attempts have been made to improve the adhesion between the components using commercial chain extenders (CE) as well. Chain extenders are molecules with functional properties that reconnect polymer chains that have broken due to degradation. The functional groups of these extender molecules are reactive with hydroxyl, carboxyl and isocyanate groups making it a promising connector between TPS and PLA. Zhang et al. [14] observed that the presence of CE facilitates a better dispersion of components and enhances the compatibility between the PLA and TPS. It was also pointed out [15] that CE only causes a marginal improvement when used together with MA-based compatibilization.

Unfortunately, the mechanical properties of the TPS component drastically depend on the humidity, plasticizer type/content and the processing parameters. Therefore, a wide range of tensile strength (0.4–38 MPa) and elongation at break (1–129%) values can be found in the literature [4]. Accordingly, the results obtained by the different studies regarding the effects of various coupling agents are difficult to compare.

Here, PLA/TPS blends were prepared *via* batchwise melt mixing with and without reactive compatibilization. Firstly, blends with different PLA/TPS ratios were prepared and characterized. Subsequently the sample containing 75 wt% PLA and 25 wt% TPS was prepared with different chemical connectors: (i) maleic anhydride with dicumyl peroxide as grafting initiator, (ii) blocked isocyanate and (iii) chain extender (multifunctional oligomer). The paper focuses on the assessment of mechanical, morphological and thermal properties of the prepared blends.

2. Experimental

2.1. Materials

The TPS was produced with native maize starch (Hungramid F Meritena 100) supplied by Brenntag Ltd (Budapest, Hungary). As plasticizers of starch glycerol and distillated water was used. The glycerol (purity of 99.5%) was obtained from a local supplier (Csepp Bt.; Budapest, Hungary). Stearic acid obtained from ICC Chemol Ltd. (Budapest, Hungary) was used as lubricant when processing TPS. The PLA (Ingeo 3052D) was obtained from NatureWorks LLC (Minnetonka, USA).

The MA was purchased from Sigma-Aldrich Chemie GmbH (Munich, Germany). The DCP (Retic DCP 40 MG) was obtained from Oxido s.r.l. (Anagni, Italy). Commercially available CE (Joncryl ADR®-4368C) was supplied by BASF SE (Ludwigshafen, Germany). The blocked isocyanate (Trixene BI 7963) - hexamethylene diisocyanate blocked with diethyl malonate (bHDI) - was purchased from Lanxess Urethanes UK Ltd. (Accrington, UK).

2.2. Processing of the materials

Prior to processing the maize starch was conditioned in a Memmert HCP153 humidification chamber (Frankfurt, Germany) at 30 °C and a relative humidity (RH) of 50% for 24 h. Subsequently, the starch, the plasticizers and the lubricant were weighed according to Table 1 and premixed manually to obtain a "dry mixture".

Table 1. The recipe of the TPS

Starch [wt%]	Glycerol [wt%]	Distilled water [wt%]	Stearic acid [wt%]
66	16.5	16.5	1

The prepared "dry mixture" was melt-compounded in a Labtech LTE 26-44 type twin-screw extruder (Samutprakan, Thailand) with a screw diameter of 26 mm and L/D ratio of 44. The heating zones of the extruder barrel were maintained at a temperature of 85, 90, 95, 100, 100, 100, 110, 110, 120, 120 °C from feed zone to die end, respectively. The screw speed was set to 75 rpm. Starve feeding of the extruder was done manually. The extruder barrel was equipped with an atmospheric vent to remove the vaporized water. After the melt compounding, the obtained TPS was pelletized.

Prior to the blending of the components the TPS granules were conditioned at 30 °C and 50% RH for 24 h, while the PLA pellets were dried in a drying chamber at 80 °C for 4 h. The PLA/TPS blends were produced in a Brabender Plasti-Corder

PL2000 type kneading chamber (Duisburg, Germany). The screw speed was set to 50 rpm, the temperature of the mixing chamber was 170 °C. Table 2 shows the composition of the prepared mixtures. The amount of coupling agents introduced was an average value determined based on the literature [4].

Table 2. The recipe of the PLA/TPS blends

Sample	PLA [wt%]	TPS [wt%]	DCP [phr]	MA [phr]	bHDI [phr]	CE [phr]
PLA	100	-	-	-	-	-
PLA/TPS25	75	25	-	-	-	-
PLA/TPS50	50	50	-	-	-	-
PLA/TPS75	25	75	-	-	-	-
TPS	-	100	-	-	-	-
PLA/TPS_MA	75	25	0.25	2.5	-	-
PLA/TPS_bHDI	75	25	-	-	2.5	-
PLA/TPS_CE	75	25	-	-	-	0.5

In the next step, all the prepared blends were compression molded into sheets of 1.25 mm thickness in a Collin Teach-Line Platen Press 200E hot press machine (Munich, Germany) at the temperature of 170 °C and a pressure of 25 bar for 5 mins. Specimens for testing were cut out of the compression molded sheets with a Mutronic Diadisk cutter (Rieden, Germany).

2.3. Characterization

Samples were conditioned under the same circumstances (30 °C, 50% RH) for at least 48 h prior to the tests in order to obtain reproducible results.

The mechanical properties were determined by tensile tests performed on a universal testing machine (Zwick Z020, Ulm, Germany) equipped with a 20 kN sensor at a tensile speed of 5 mm/min. Specimen type: 3 according to EN ISO 8256 were used for tensile tests. The tests were performed at room temperature. The average values were derived from five parallel measurements.

A scanning electron microscope (SEM) JEOL JSM 6380LA (Tokyo, Japan) was used to observe the fracture surfaces of the PLA/TPS blends. Prior to their inspection, the samples were sputter-coated with gold/palladium alloy.

Thermogravimetric analysis (TGA) was performed with a TGA Q500 analyzer (TA Instruments, New Castle, New Jersey, USA) to examine the thermal stability of the samples. Tests were carried out by heating up samples of 4 ± 1 mg from room temperature to 500 °C at a heating rate of 10 °C min^{-1} under nitrogen purge with a flow rate of 60 ml/min.

3. Results and discussion

3.1. Tensile mechanical properties

The tensile mechanical properties of non-compatibilized PLA/TPS blends are summarized in Fig. 1. It can be observed that PLA has a significantly higher yield strength (50 MPa > 10 MPa) and Young's modulus (1.9 GPa > 1.3 GPa) than TPS. Interestingly, with respect to elongation at yield point PLA also outperforms TPS (4.0% > 0.9%). This indicates that TPS has a rigid behavior, which can be attributed to the relatively high processing temperature. The mechanical properties of the PLA/TPS blends show a minimum at 75 wt% TPS content. Presumably at this point TPS can be considered as the continuous phase, which contains PLA segments acting as failure sites. These results also refer to a poor adhesion between the components and are in good agreement with the corresponding literature [16].
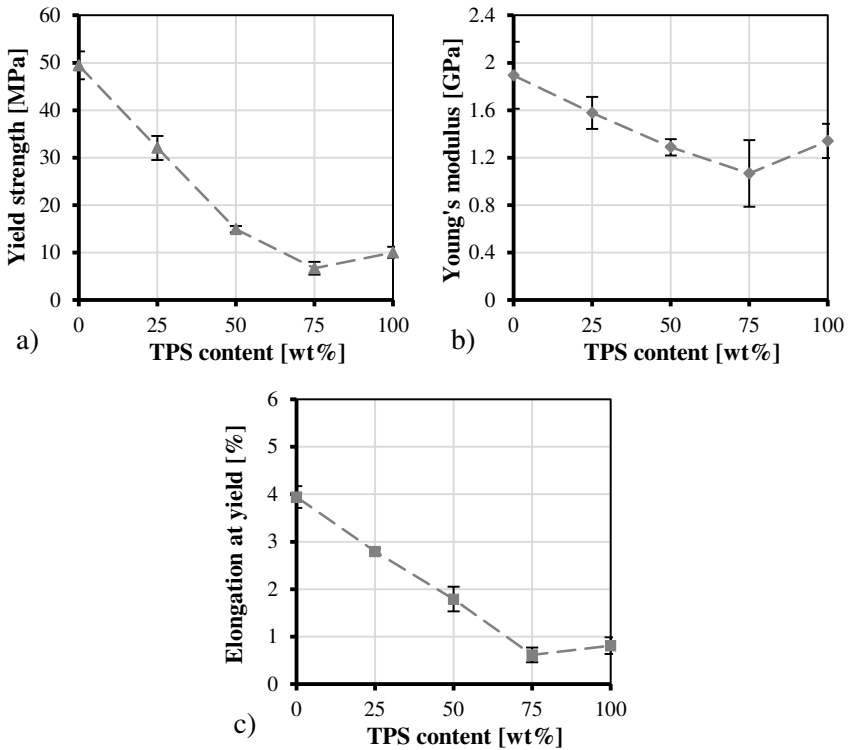

Figure 1. Yield strength (a), Young's modulus (b) and elongation at yield (c) of PLA/TPS blends as a function of TPS content

The tensile mechanical properties of the compatibilized blends containing 75 wt% PLA and 25 wt% TPS compared to the non-compatibilized PLA/TPS25 sample are shown in Fig. 2. It can be observed, that all type of coupling agents increased the elongation of the PLA/TPS blend relatively by ~20% (from 27% to ~32%). In the meanwhile, the changes in tensile strength differ depending on the type of the coupling agent introduced. The strength of the MA-compatibilized blend was similar to that of neat PLA/TPS25, however, using bHDI as additive decreased it slightly. After CE was added the strength increased from 32 MPa to 38 MPa, which could be attributed to the improved adhesion between the components. The changes in Young's modulus were within the deviation range in each case.
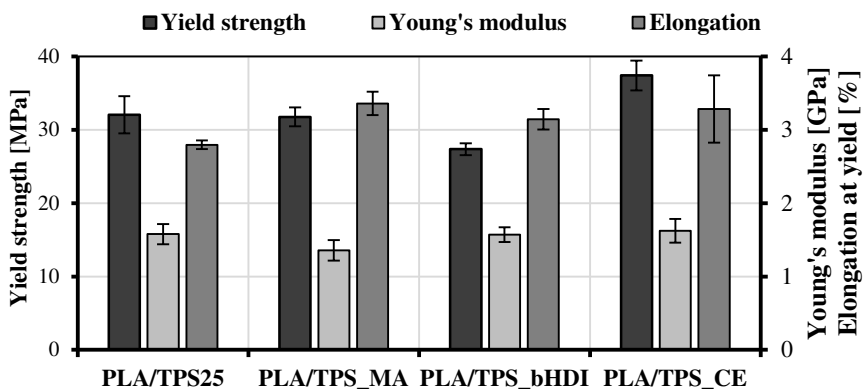

Figure 2. Yield strength, Young's modulus and elongation at yield of the samples PLA/TPS25, PLA/TPS_MA, PLA/TPS_bHDI and PLA/TPS_CE

3.2. Morphological properties

Fig. 3 reveals the SEM images of the samples PLA, TPS and PLA/TPS50. Fig. 3a and 3b show that both TPS and PLA have a homogenous, rigid fracture surface. Conversely, the blend in between reveals an inhomogeneous surface with cracks and cavities. Fig. 3c substantiates the assumption made based on the mechanical results, namely, that the adhesion between the two components is rather poor.
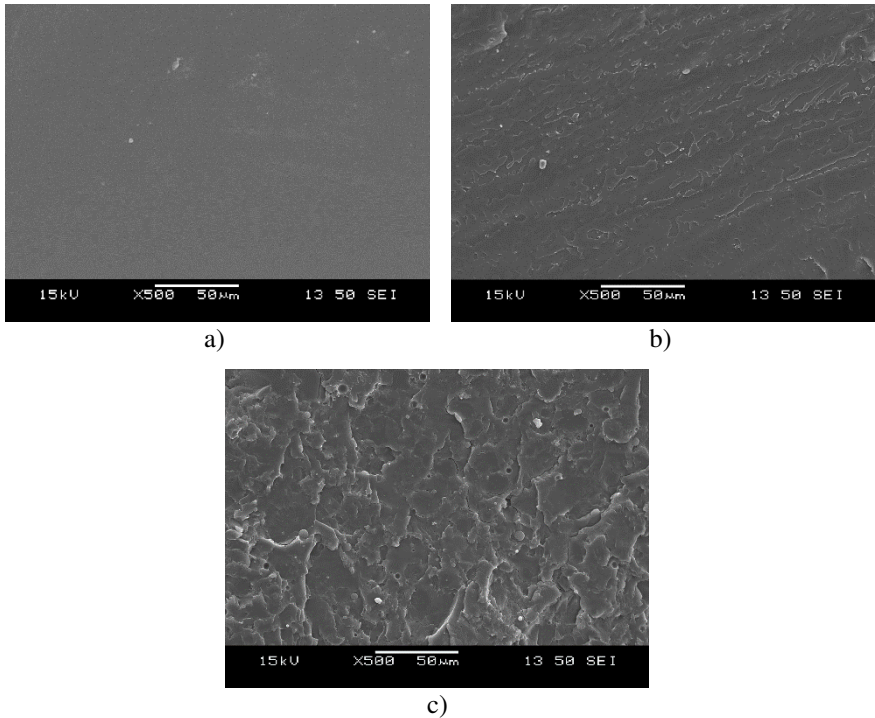
a)

b)

c)

Figure 3. SEM images of the samples TPS (a), PLA (b) and PLA/TPS50 (c)

Fig. 4 shows the SEM images taken of the fracture surface of the PLA/TPS25 sample and its compatibilized variants. The PLA/TPS25 sample shows an inhomogenous characteristics, similar to PLA/TPS50. The fracture surfaces of compatibilized blends are also inhomogeneous, however in these cases little to no stress fractures, cavities or cracks can be observed. Also, the interface between the components seems much more stable and homogenous. These conclusions are in good accordance with the increased elongation values that were measured during the tensile tests.
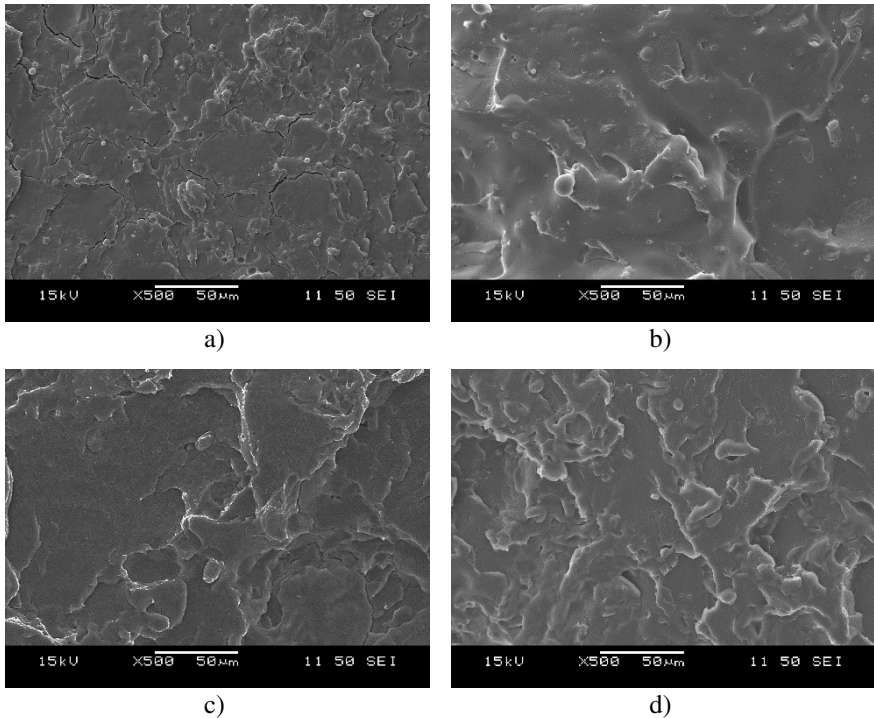
a)

b)

c)

d)

Figure 4. SEM images of the samples PLA/TPS25 (a) PLA/TPS_MA (b),
PLA/TPS_bHDI (c) and PLA/TPS_CE (d).

3.3. TGA behavior

Fig. 5a shows the TGA traces, whereas Fig. 5b shows its derivatives (DTG) for PLA, TPS and the neat PLA/TPS blends. According to the literature, the thermal decomposition of TPS components takes place below 350 °C, while the thermal degradation processes observed above 350 °C are related to the PLA [9]. The TPS containing samples underwent a two-step degradation. The first transition that can be observed between 50-250 ° C is related to the elimination of water, glycerol and other low molecular weight compounds [17]. The second – and more significant – transition is related to the thermal decomposition of TPS. The neat PLA decomposed in one step at ~360 °C.
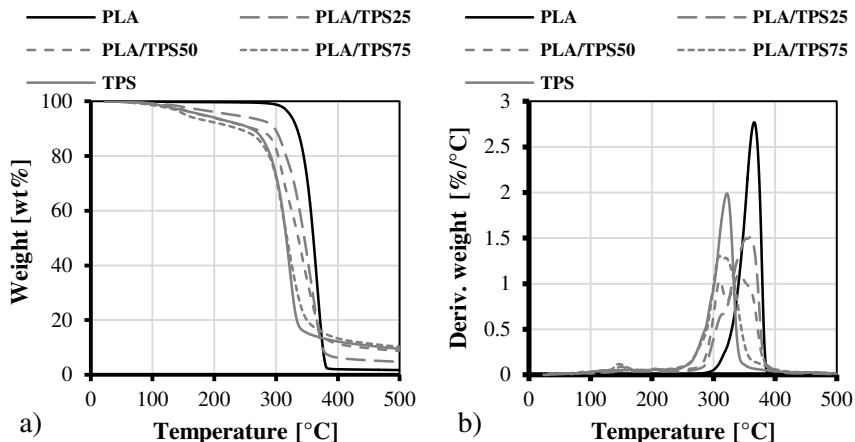
Figure 5. TGA (a) and DTG (b) curves of PLA, TPS and the non-compatibilized PLA/TPS blends

Table 3 lists the temperature values derived from the TGA curves corresponding to 10, 25, 50, 75% mass losses. Besides, the maximum values of peaks appearing in DTG curves corresponding to the degradation of TPS (T_{pTPS}) and PLA (T_{pPLA}), and the residual mass (char) is also listed. Based on the data it can be assumed that blending PLA with TPS decreases the thermal stability of both components. The char formation (residual mass) at higher temperature was mostly due to the TPS phase.

Table 3. TGA data determined for PLA, TPS and the non-compatibilized PLA/TPS blends

Sample	T_{10} [°C]	T_{25} [°C]	T_{50} [°C]	T_{75} [°C]	T_{pTPS} [°C]	T_{pPLA} [°C]	Resid. [wt%]
PLA	334	348	360	369	-	366	1.8
PLA/TPS25	298	323	346	363	314	360	4.5
PLA/TPS50	264	309	336	360	310	342	8.8
PLA/TPS75	248	297	318	340	315	329	10.3
TPS	252	295	315	329	322	-	10.1

The effect of different compatibilizers on the thermal stability of PLA/TPS blends were also examined. The TGA and DTG curves are shown in Fig. 6a and Fig 6b, respectively. It can be observed that the presence of MA and bHDI does not change the thermal stability of PLA/TPS blends significantly. The CE, however, increased all the T-values by 2-6 °C.
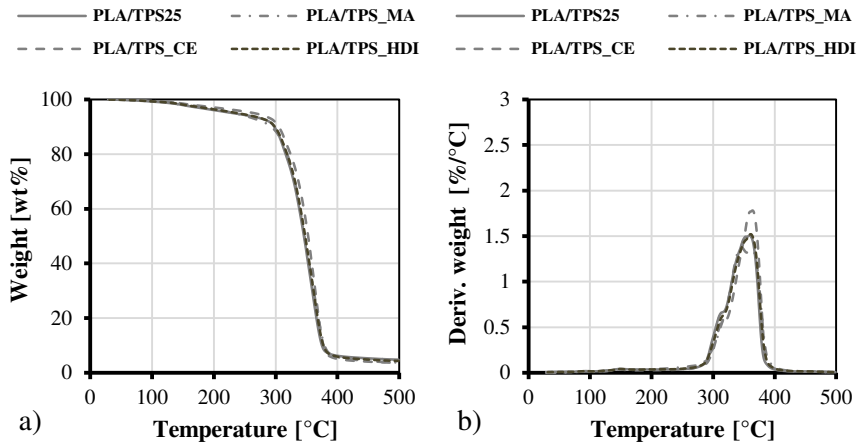
Figure 6. TGA (a) and DTG (b) curves of PLA/TPS25 and its compatibilized variants

The related data are summarized in Table 4.

Table 4. TGA data of the PLA/TPS25 blend and its compatibilized variants

Sample	T_{10} [°C]	T_{25} [°C]	T_{50} [°C]	T_{75} [°C]	T_{pTPS} [°C]	T_{pPLA} [°C]	Resid. [wt%]
PLA/TPS25	298	323	346	363	314	360	4.5
PLA/TPS_MA	293	325	347	365	318	362	3.8
PLA/TPS_bHDI	299	326	347	365	315	359	4.0
PLA/TPS_CE	305	331	352	367	317	366	3.7

4. Conclusions

The effect of three different coupling agents (namely MA, bHDI and CE) on PLA/TPS blends were examined in this study. The results of the mechanical and morphological tests showed that blends consisting of neat PLA and TPS exhibit a rather poor interfacial adhesion. According to the SEM images all three chemical connectors improved the adhesion between the components leading to a stable, homogenous fracture surface. However, the improvement in tensile mechanical properties were marginal. Out of the three examined coupling agents the CE proved to be the most effective, even though it was the one being introduced in the smallest amount (0.5 wt%). The samples that contained CE exhibited a ~20% higher yield strength and elongation than the neat PLA/TPS at constant Young's modulus. The TGA tests showed that MA and bHDI does not affect the thermal stability of the blends, the CE however increases it slightly.

Acknowledgement

References

[1] R. F. T. Stepto, Thermoplastic Starch, Macromolecular Symposia 279 (1) (2009) pp. 163-168.
doi: *https://doi.org/10.1002/masy.200950525*

[2] H. Liu, F. Xie et al., Thermal processing of starch-based polymers, Progress in Polymer Science 34 (12) (2009) pp. 1348-1368.
doi: *https://doi.org/10.1016/j.progpolymsci.2009.07.001*

[3] T. Singh, B. Gangil et al., Agriculture waste reinforced corn starch-based biocomposites: effect of rice husk/walnut shell on physicomechanical, biodegradable and thermal properties, Materials Research Express 6 (4) (2019) 045702.
doi: *https://doi.org/10.1088/2053-1591/aafe45*

[4] J. Muller, C. Gonzalez-Martinez, A. Chiralt, Combination of Poly(lactic) Acid and Starch for Biodegradable Food Packaging, Materials 10 (8) (2017) 952.
doi: *https://doi.org/10.3390/ma10080952*

[5] M. Gáspár, Z. Benkő et al., Reducing water absorption in compostable starch-based plastics, Polymer Degradation and Stability 90 (3) (2005) pp. 563-569.
doi: *https://doi.org/10.1016/j.polymdegradstab.2005.03.012*

[6] L. Lendvai, A. Apostolov, J. Karger-Kocsis, Characterization of layered silicate-reinforced blends of thermoplastic starch (TPS) and poly(butylene adipate-co-terephthalate), Carbohydrate Polymers 173 (2017) pp. 566-572.
doi: *https://doi.org/10.1016/j.carbpol.2017.05.100*

[7] D. Garlotta, A Literature Review of Poly(Lactic Acid), Journal of Polymers and the Environment 9 (2) (2001) pp. 63-84.
doi: *https://doi.org/10.1023/A:1020200822435*

[8] L. Kotrocz, P. Bakonyi, Pinpoint Loading Examinations of Poly(lactic acid) Biopolymers, Acta Technica Jaurinensis 11 (4) (2018) pp. 206-217.
doi: *https://doi.org/10.14513/actatechjaur.v11.n4.480*

[9] N. A, X. Li et al., Starch/polylactide sustainable composites: Interface tailoring with graphene oxide, Composites Part A: Applied Science and

Manufacturing 69 (0) (2015) pp. 247-254.
doi: *http://dx.doi.org/10.1016/j.compositesa.2014.11.025*

[10] R. Acioli-Moura, X. S. Sun, Thermal degradation and physical aging of poly(lactic acid) and its blends with starch, Polymer Engineering and Science 48 (4) (2008) pp. 829-836.
doi: *https://doi.org/10.1002/pen.21019*

[11] Z. Xiong, L. S. Zhang et al., Effect of castor oil enrichment layer produced by reaction on the properties of PLA/HDI-g-starch blends, Carbohydrate Polymers 94 (1) (2013) pp. 235-243.
doi: *https://doi.org/10.1016/j.carbpol.2013.01.038*

[12] M. A. Huneault, H. Li, Morphology and properties of compatibilized polylactide/thermoplastic starch blends, Polymer 48 (1) (2007) pp. 270-280.
doi: *https://doi.org/10.1016/j.polymer.2006.11.023*

[13] V. H. Orozco, W. Brostow et al., Preparation and Characterization of Poly(Lactic Acid)-g-Maleic Anhydride + Starch Blends, Macromolecular Symposia 277 (1) (2009) pp. 69-80.
doi: *https://doi.org/10.1002/masy.200950309*

[14] Y. C. Zhang, X. Yuan et al., The Effect of Polymeric Chain Extenders on Physical Properties of Thermoplastic Starch and Polylactic Acid Blends, Journal of Polymers and the Environment 20 (2) (2012) pp. 315-325.
doi: *https://doi.org/10.1007/s10924-011-0368-3*

[15] H. Li, M. A. Huneault, Effect of chain extension on the properties of PLA/TPS blends, Journal of Applied Polymer Science 122 (1) (2011) pp. 134-141.
doi: *https://doi.org/10.1002/app.33981*

[16] M. L. Sanyang, S. M. Sapuan et al., Development and characterization of sugar palm starch and poly(lactic acid) bilayer films, Carbohydrate Polymers 146 (2016) pp. 36-45.
doi: *https://doi.org/10.1016/j.carbpol.2016.03.051*

[17] A. Ujcic, M. Nevoralova et al., Thermoplastic Starch Composites Filled With Isometric and Elongated TiO2-Based Nanoparticles, Frontiers in Materials 6 (284) (2019)
doi: *https://doi.org/10.3389/fmats.2019.00284*

Stability Analysis of an Assembly Process Using Simulation

L. Rónai[1,*], T. Szabó[1]

[1]University of Miskolc, Robert Bosch Department of Mechatronics
Egyetemváros, 3515 Miskolc, Hungary
e-mail: ronai.laszlo@uni-miskolc.hu

Abstract: This paper deals with an assembly process of batteries with cell holder. The operation involves snap-fitting phenomenon, which is a mechanical stability problem. The structure of the cell holder is modelled with 2D flexible beam elements assuming large displacements. The stability of the equilibrium is investigated taking into consideration non-frictional and Coulomb frictional contacts. The goal of the analysis to determine the boundary point of the feed-motion from which the battery snaps-in to the final assembled position autonomously. The effect of the velocity of the battery feed-motion is also considered with energy approach.

Keywords: *stability; nonlinear structure; friction; snap-fit*

1. Introduction

Snap-fit elements [1] [2] [3] [4] are frequently applied in toy industry and also in daily used equipment. These products are assembled using human force with the help of human touch [5]. A man can sense the occurrence of the snap-fit if the process is carried out. Industrial robots are usually equipped with position control only, but it can be enhanced with machine haptic feedback [6]. Robotic assembling tasks, which involve snap-fit elements require their stability analysis in order to protect from overloading the workpiece and the robot. Another requirement is to minimize the execution time of assembling.

The stability of mechanical equilibrium containing only conservative forces can be discussed with the Lagrange-Dirichlet theorems [7] [8]. When dissipative forces are also present the Salvadori's theorem is applicable [8]. Considering friction adhesion also may take place.

Finite Element Method (FEM) can be applied to analyse elastic structures for static and dynamic problems [9] [10] [11]. Nonlinear structures including frictions can be modelled also with FEM. The snap-fit elements are flexible structures, which can be represented with slender beam elements assuming large displacements and small deformations. A nonlinear analysis of the snap-fit can be performed by the help of Updated Lagrangian description [12] or corotational approach [13]. In ideal circumstances normal contact takes place between the contacting bodies but in real life problems the friction cannot be neglected. In this paper a quasi-static and dynamic insertion of a battery into a plastic cell holder is investigated without friction and with Coulomb friction. Snap-fit phenomenon takes place at instable equilibrium position. A numerical method is proposed in this paper to determine a so-called pre-instability position in case of dynamic assembly.

The rest of the paper is organized as follows: Section 2 describes the stability analysis of the non-friction and friction contact models. Concluding remarks are summarized in Section 3.

2. Stability analysis of the assembling process

Assembling operation of a battery into a cell holder by an industrial robot is shown in Fig. 1. The battery is modelled as a rigid body and the cell holder is a flexible beam structure. The diameter of the battery is 18 mm and its mass is m=0.0458 kg.
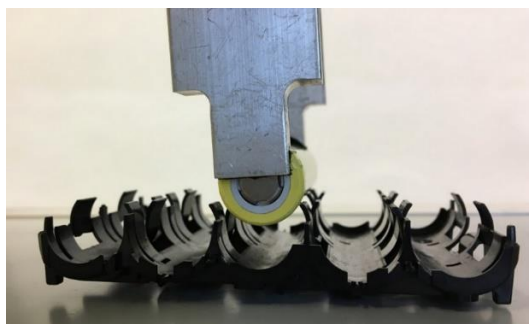
Figure 1. Assembling of a battery into a cell holder

The symmetric geometry of the curved beam structures is shown in Fig. 2. The curved beams of the cell holder consist of two arches with equal radius R=9 mm and the angles are 1 rad and 0.63 rad. The cross section of the beam area is A=18.25 mm^2 and the moment of inertia of cross section is I=1.52 mm^4. The material of the cell holder is Acrylonitrile Butadiene Styrene (ABS) and the Young's modulus is 2.415 GPa. One branch of the cell holder subdivided into 20 uniform beam elements.
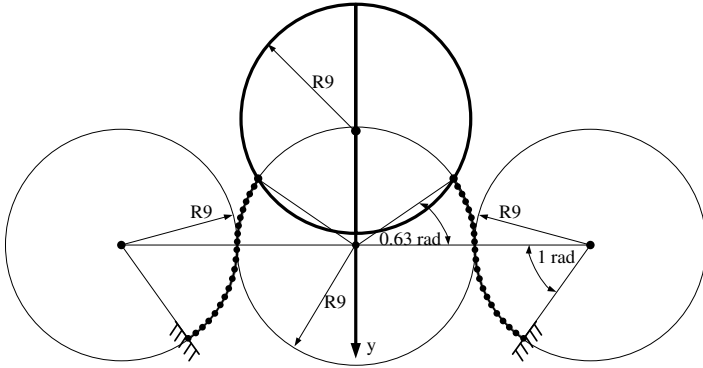
Figure 2. 2D geometry of the battery and cell holder

A special purpose nonlinear finite element program has been developed under Scilab system in order to analyse the feed-motion of the battery [6].
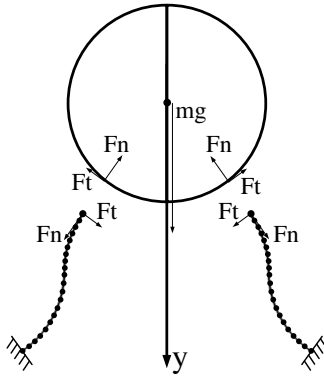

Figure 3. Free body diagram of the contact forces

The equilibrium iteration $s = 1, 2, 3, ...,$ is performed by Newton-Raphson method

$$^{t+\Delta t}\widehat{\mathbf{K}}_{\mathbf{t}}^{(s)}\Delta\mathbf{q}^{(s)} = {}^{t+\Delta t}\mathbf{f}_{\mathbf{u}}^{(s)} - {}^{t+\Delta t}\mathbf{f}_{\mathbf{c}}^{(s-1)} - {}^{t+\Delta t}\widehat{\mathbf{f}}_{\mathbf{i}}^{(s-1)}, \tag{1}$$

where $^{t+\Delta t}\widehat{\mathbf{K}}_{\mathbf{t}}^{(s)}$ is the tangential stiffness matrix, $^{t+\Delta t}\mathbf{f}_{\mathbf{u}}^{(s)}$ is the kinematical load vector, $^{t+\Delta t}\mathbf{f}_{\mathbf{c}}^{(s-1)}$ is the force vector due to contact, $^{t+\Delta t}\widehat{\mathbf{f}}_{\mathbf{i}}^{(s-1)}$ is the internal load vector, and $\Delta\mathbf{q}^{(s)}$ is the vector of the displacement increments. The associated vectors and matrices of the finite elements are published in [6]. It is noted that the beam elements suffer large displacements and small deformations.

The program determines the contact forces (see Fig. 3) in the course of feed-motion. The assembly force is the sum of the vertical projections of the normal and tangential contact forces F_n, F_t. It is noted that in non-friction case $F_t = 0$.

2.1. Modelling with non-friction contact

The computed assembly force assuming frictionless operation is shown in Fig. 4. The feed-motion denotes the vertical displacement of the battery. The maximum displacement is 10.05 mm and it was performed by 30 uniform increments. The weight of the battery 0.449298 N is represented by horizontal thin solid line. The robotic assembly is performed very slowly, which can be regarded as a quasi-static motion. The goal is to find equilibrium position having instability, where only the gravity is exerted on the battery and for any arbitrary small disturbance it moves autonomously to the assembled position. The intersection of the curve of the load versus feed-motion and the weight of the battery provide two equilibrium points.
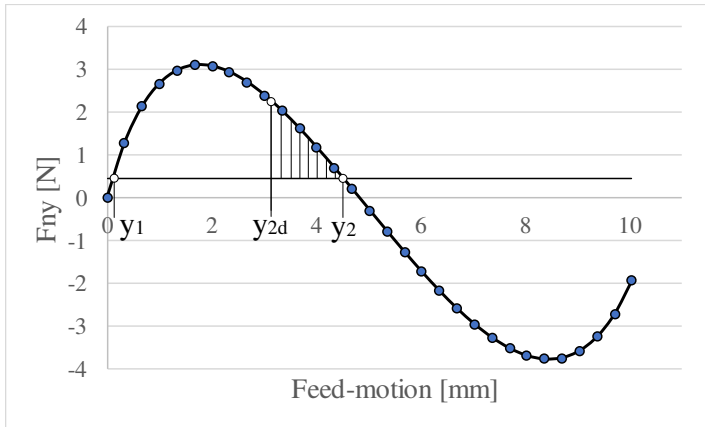

Figure 4. Insertion load versus feed-motion of the battery

The first equilibrium point is at $y_1 = 0.1178\ mm$, the second one is at $y_2 = 4.52552\ mm$. In accordance with Lagrange-Dirichlet method the criteria of the stability is $\delta\Pi = 0$ and $\delta^2\Pi > 0$, where Π is the potential energy of the system.

The potential energy is written as

$$\Pi = U - mgy, \tag{2}$$

where U is the strain energy of the flexible cell holder.

The first variation of the potential energy as follows

$$\delta\Pi = 0 = \frac{\partial U}{\partial y}\delta y - mg\delta y = \left(\frac{\partial U}{\partial y} - mg\right)\delta y, \tag{3}$$

where $\frac{\partial U}{\partial y} = F_{ny}$ represents the vertical projection of the internal force, which is equal to mg at the equilibrium positions.

Taking of the second variation of the potential energy

$$\delta^2\Pi = \frac{\partial^2 U}{\partial y^2}(\delta y)^2 = \frac{\partial F_{ny}}{\partial y}(\delta y)^2, \tag{4}$$

where $\frac{\partial F_{ny}}{\partial y} > 0$ at $y_1 = 0.1178 \, mm$ and $\frac{\partial F_{ny}}{\partial y} < 0$ at $y_2 = 4.52552 \, mm$ according to Fig. 4. Therefore, the first equilibrium point is stable and the second one is unstable. It means that if the end-effector of the robot is opened a bit over the second point, the battery would snap-in.

Usually the assembling operation is performed dynamically, which means that when the gripper is opened the battery has an initial velocity, e.g., in teach mode of the robot its magnitude $v_0 = 0.25 \, m/s$. Therefore, the gripper can be opened earlier at y_{2d} called as pre-instable position, and its kinetic energy can cover the strain energy increment, which is equal to the area of the triangle shown in Fig. 4:

$$\frac{1}{2}mv_0^2 = \int_{y_{2d}}^{y_2} F_{ny} \, dy - mg(y_2 - y_{2d}), \tag{5}$$

where

$$\int_{y_{2d}}^{y_2} F_{ny} \, dy = \int_0^{y_2} F_{ny} \, dy - \int_0^{y_{2d}} F_{ny} \, dy \cong I_F(y_2) - I_F(y_{2d}), \tag{6}$$

$I_F(y)$ is the integral of the internal force computed numerically shown in Fig. 5.
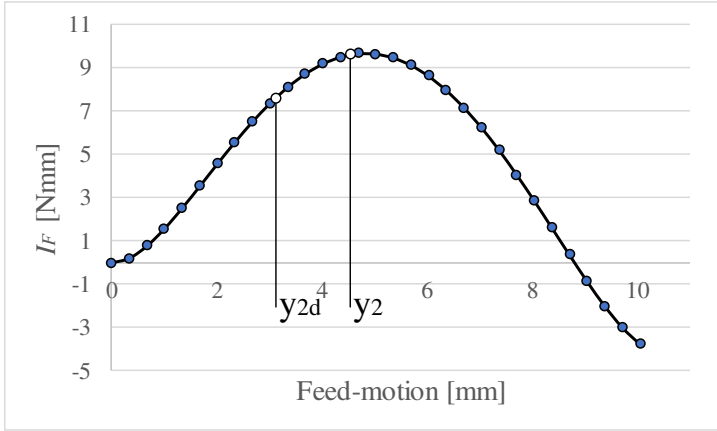
Figure 5. Numerically integrated internal force

Substituting (6) into (5) $I_F(y_{2d})$ can be expressed as:

$$I_F(y_{2d}) \cong I_F(y_2) - \frac{1}{2}mv_0^2 - mg(y_2 - y_{2d}), \tag{7}$$

the position y_{2d} can be obtained by the inverse function of $I_F(y)$:

$$y_{2d} \cong I_F^{-1}(I_F(y_{2d})). \tag{8}$$

Solving numerically the implicit equation (7) $y_{2d} \cong 3.07\ mm$. The opening command of the end-effector can be initiated by the robot when the battery is arrived at the y_{2d} position then it will snap-in to its assembled position. It means that the dynamical feed-motion of the battery shorten the feed-motion and the assembling time at the same time.

2.2. Modelling with friction

Friction is always present in practical contact problems. Therefore, to take it into consideration in the assembling operation of the battery is obvious. Assuming Coulomb dry sliding friction the coefficient is taken to $\mu = 0.15$ between the cell holder and the plastic-coated battery during feed-motion. It means that according to Fig. 3

$$F_t = \mu F_n. \tag{9}$$

When the feed-motion is stopped in an equilibrium position adhesion may takes place in state of stability or sliding (9) in case of instability.
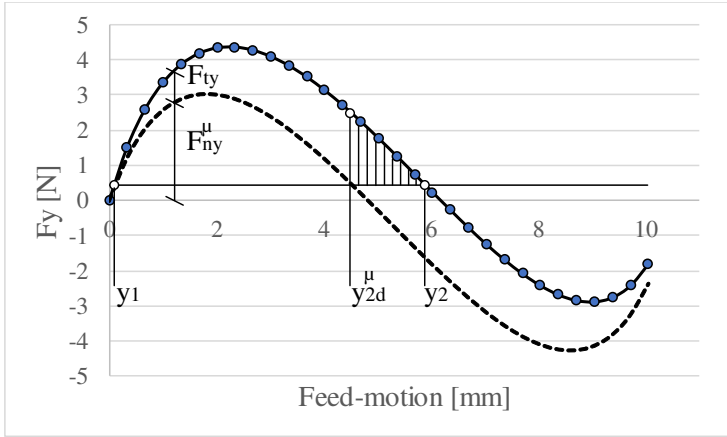
Figure 6. Load versus feed-motion curve considering friction

The vertical components of the tangential F_{ty} and normal F_{ny}^{μ} contact forces have been computed by the nonlinear FEM program considering Coulomb friction (9). The results are shown in Fig. 6. It is noted that the curve of the normal contact force F_{ny}^{μ} though it is like the curve F_{ny} in Fig. 4 but not equal because the principle of the superposition is not applicable for nonlinear problems. The assembly force can be obtained by the projection of the normal and tangential contact forces:

$$F_y = F_{ty} + F_{ny}^{\mu}. \tag{10}$$

There are also two equilibrium positions obtained by the weight of the battery. In the first equilibrium position at y_1 stick takes place and the system can be regarded to be conservative and can be treated as in Section 1.1. The second one at $y_2 = 5.95 \, mm$ is a candidate point for the snap-fit. However, the investigated system is non-conservative due to friction. The stability of a non-conservative mechanical systems can be analysed by Salavadori's theorem.

Theorem 1 (L. Salvadori [1966] ref. [8]):

Hypothesis (i)   If the potential energy Π has a minimum at $q = 0$;

Hypothesis (ii)   the equilibrium at $q = 0$ is isolated;

Hypothesis (iii)   the dissipation is complete, i.e., for some function $a \in \mathcal{K} : (Q|\dot{q}) \leq -a(\|\dot{q}\|)$.

Then the equilibrium $q = \dot{q} = 0$ is asymptotically stable.

If the first Hypothesis (i) is replaced by the condition (i-a) Π has no minimum at $q = 0$ then the equilibrium $q = \dot{q} = 0$ is unstable.

As it was noted previously, the equilibrium position at y_2 is a candidate for instability. Therefore, the (i-a) condition will be investigated. The notations of the theorem are given as follows $q = y - y_2$, $\dot{q} = \dot{y}$ and $Q = F_t$, noting that $\dot{q}$ and F_t have opposite signs.

The potential energy of the conservative gravity and internal forces:

$$\Pi = U - mgq. \tag{11}$$

The first derivative of the potential energy is written

$$\left.\frac{\partial \Pi}{\partial q}\right|_{q=0} = \frac{\partial U}{\partial q} - mg, \tag{12}$$

where $\frac{\partial U}{\partial q} = \frac{\partial U}{\partial y} = F_{ny}^{\mu}$ denoted by dashed line in Fig. 6 and its value is equal to - 1.625 N, i.e.,

$$\left.\frac{\partial \Pi}{\partial y}\right|_{y=y_2} = F_{ny}^{\mu} - mg = -1.625 - 0.4493 \neq 0. \tag{13}$$

The instability of the candidate position y_2 is proved mathematically according to Hypothesis (i-a).

Due to dynamic feed-motion $v_0 = 0.25 \ m/s$ the gripper can be opened before the battery arrives at position y_2 also in case of friction. The determination of the pre-instable position y_{2d}^{μ} is performed by a similar method, which was detailed in non-friction contact model.

$$\frac{1}{2}mv_0^2 = \int_{y_{2d}^{\mu}}^{y_2} F_y \, dy - mg\left(y_2 - y_{2d}^{\mu}\right), \tag{14}$$

where

$$\int_{y_{2d}^{\mu}}^{y_2} F_y \, dy = \int_0^{y_2} F_y \, dy - \int_0^{y_{2d}^{\mu}} F_y \, dy \cong I_F^{\mu}(y_2) - I_F^{\mu}(y_{2d}^{\mu}), \tag{15}$$

$I_F^{\mu}(y)$ is the numerically computed integral of the internal force shown in Fig. 7.
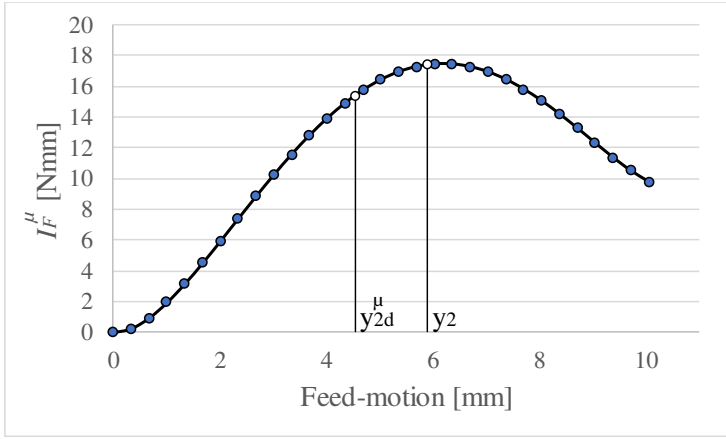
Figure 7. Numerically integrated internal force considering friction

Substituting (15) into (14) the integral of the internal force at position y_{2d}^{μ} is given as

$$I_F^{\mu}\left(y_{2d}^{\mu}\right) \cong I_F^{\mu}(y_2) - \frac{1}{2}mv_0^2 - mg\left(y_2 - y_{2d}^{\mu}\right), \tag{16}$$

y_{2d}^{μ} can be determined from (8) by iteration. The gripper can be opened at position $y_{2d}^{\mu} = 4.522 \ mm$ earlier than y_2.

3. Conclusions

Stability analysis of a nonlinear system containing battery and cell holder has been described in this paper. Two equilibrium positions were investigated with non-friction and friction contact models. The flexible elastic nonlinear structure was modelled with slender beam FEM elements.

Stable and unstable equilibrium positions have been determined assuming quasi static feed-motion. The latter one produces snap-fit phenomenon, where a robot gripper can be opened, then the assembly is performed autonomously.

An approximate method is proposed in this paper to determine a pre-instable position before the equilibrium is reached. It is shown that the distance of the feed-motion can be decreased when the kinetic energy of the battery is not neglected, i.e., dynamical assembly is performed with a given velocity.

Acknowledgement

References

[1]   BASF Corporation, Snap-Fit Design Manual (2007) [cited 2020-01-04] URL *www.plasticsportal.com/usa*

[2]   BAYER Materialscience LLC, Snap-Fit Joints for Plastics, A design Guide, Bayer Polycarbonates Business Unit, Pittsburg, Pennsylvania, 1998.

[3]   C. Klahn, D. Singer, M. Meboldt, Design Guidelines for Additive Manufactured Snap-Fit Joints, Procedia CIRP 50 (2016) pp. 264–269. doi: *https://doi.org/10.1016/j.procir.2016.04.130*

[4]   R. M. Kshirsagarl, D. B. Pawar, Design and analysis of snap fit joint in plastic part, International Journal of Innovative and Emerging Research in Engineering 2 (1) (2015) pp. 83–87.

[5]   M. Radi, G. Reinhart: Industrial Haptic Robot Guidance System for Assembly Processes, IEEE Conference, Lecco, Italy, 2009, pp.1–6. doi: *https://doi.org/10.1109/HAVE.2009.5356135*

[6]   L. Rónai, T. Szabó, Snap-fit Assembly Process with Industrial Robot Including Force Feedback, Robotica, Cambridge University Press 38 (2) (2020) pp.317–336. doi: *https://doi.org/10.1017/S0263574719000614*

[7]   Gy. Béda, I. Kozák, Mechanics of elastic bodies, Műszaki könyvkiadó, Budapest, 1987, in Hungarian.

[8]   N. Rouche, P. Habets, M. Laloy, Stability Theory by Liapunovs Direct method, Springer-Verlag, New York, 1977.

[9]   L. Fehér L, J. Égert, FEM Modeling and Weight Reduction of a Solar Energy
      Driven Racing Car Chassis, Acta Technica Jaurinensis 8 (4) (2015) pp. 296–
      311.
      doi: *https://doi.org/10.14513/actatechjaur.v8.n4.385*

[10] J. Égert, Finite Element Mechanical Modeling Opportunities in Machine
      Design, Acta Technica Jaurinensis 1 (1) (2008) pp. 47–59.

[11] P. Horváth, J. Égert, Dynamic Analysis of a One-cylinder Engine Crankshaft,
      Acta Technica Jaurinensis 8 (4) (2015) pp. 280–295.
      doi: *https://doi.org/10.14513/actatechjaur.v8.n4.379*

[12] K. J. Bathe: Finite Element Procedures, Prentice Hall, Upper Saddle River,
      New Jersey, 1996.

[13] M. A. Crisfield: Non-linear Finite Element Analysis of Solids and Structures,
      John Wiley and Sons, New York City, 1991.

Study on Relationship between Roles of Public Open Spaces and Pedestrians Inside Campus: Case Studies from Universities in Thailand and Hungary

C. Kongphunphin[1], P. Hegyi[2], C. Koren[2,*]

**[1]Thammasat University, Faculty of Architecture and planning
Klong luang, 12120 Pathum thani, Thailand
[2]Széchenyi István University, Department of Transport Infrastructure and
Water Resources Engineering
Egyetem tér 1, 9026 Győr, Hungary
e-mail: koren@sze.hu**

Abstract: Public open spaces in campuses are social places for students and staffs. Convenient accessibility both physical and visual is the main factor that attracts people to use these spaces. This article analyses the physical layout of public open spaces through their relationship with the surrounding. The purpose of this study is to compare the relationship between public open spaces and pedestrians in the campuses. The case study conducted in four campuses located in Thailand and Hungary. In order to get the required data, spatial analysis from Geographic Information System and observation survey was employed as qualitative techniques. The study revealed that pedestrian facilities are the most important accessibility types in public open spaces in each campus. The different lengths of pedestrian facilities are related with three factors of campuses' layout. They are the size, surrounding and design elements of the campuses and their public open spaces.

Keywords: public open space; pedestrian facilities; campus

1. Introduction

Campuses were defined as both public and semi-public spaces depending on campus access control policy. Campuses have the main role for educating and training students. There are many places inside campuses which are used not only by students and staff but also by the general public, such as a library, cafeteria, gymnasium, public open space, and so on. In any campus, its public open space is a social space with many types and functions. Public open spaces in campus are places for several activities that users can choose by themselves (for example reading, sitting, standing around, chatting, social gathering, waiting, and passing-by). In addition, there are many design elements in the spaces for promoting more convenient, safe, aesthetic, and attractive use by people. Landscapes and streetscapes design are used for developing public open spaces such as trees, fountains, lawns, planting, colourful plants, facilities)for example, benches, bins, lamps, structures and monuments(, natural views, and pedestrian facilities.

Public open space is a necessary component of campuses, but poor access to public open spaces can lead to unused areas, undesirable behaviour, strain on management, and other difficulties. In the following pages, this study analyses the relationship between roles of public open spaces and pedestrians inside campuses and their public open spaces. We analyse four campuses; they are Széchenyi István University in Gyor, Budapest University of Technology and Economics, University of Debrecen, and Thammasat University as case studies of public open spaces in campuses. First, we define the difference of layouts of the campuses. Second, we examine how to get spatial layouts and connections of open public space in the campuses. We also look at basic considerations for designing open public spaces, including comfort and convenience, visual quality, safety, and access. Much of spatial and accessible data is based on Geographic Information System)GIS(and Open Street Map)OSM(because they were the richest information available and up to date. The data from the tools is integrated with the data from sites surveying. We hope to discern the relationship between roles of public open spaces and pedestrians. There are two goals in this study stated as follows; to compare the physical layout of public spaces in the university and to compare the relationship between roles and pedestrian facilities inside the campus.

This study is a part of the doctoral thesis which topic is "An Approach to Promote Creative Urban Public Space for Sustaining Social Identity". Of course, no town is the same as another, but many share similarities. Since this research is a comparative research between Asia and Europe, the results of the study will be compared the relationship between roles of public open spaces and pedestrians inside campus with case studies from universities in Thailand and Hungary. We should identify the differences in geographical conditions, context and culture, and other situations.

These factors are causing variations of user behaviour and design of public spaces. Ultimately, the goal is to integrate knowledge and to establish recommendations for suitable public spaces in Thailand. Guidelines to build aesthetic urban environment, agreeable with urban lifestyles, will be mentioned and established. These will be recommended for implementation in the relevant sectors of urban spatial usage.

1.1. Public open spaces in campuses

Campuses can be roughly classified in two types: closed and open campus. Both are different for accessibility. Closed campuses always have office hours and the area is surrounded by fence. It is for protection and safety including a definition of the public and private zone [1][2]. Notwithstanding, building the best academic facilities is not enough to foster a well-rounded educational experience. Comfortable and lively public spaces provide informal places in and near campuses that can bring students, faculty, staff, visitors, and the community together [3]. However, public open spaces have no exact function [4][5]. They are adjustable by users. Mostly public open spaces are social places where people interact with each other [6]. They can influence physical activity in at least three ways [7]. First, public open space can be a setting where people engage in physical activities. Second, public open space can be a destination to which people actively travel either to be active or simply to socialize. Finally, public open space can be used as part of a route to pass through to reach another destination (for example, passing through a greenway to reach a shop) or as part of a recreational walk or running route. Hence public open spaces can contribute to different types of physical activities. For example, public open space as a thoroughfare is related to active travel, as a destination to either active travel or recreational physical activity, or public open space as a setting might be related to recreational walking or cycling, running, dog walking, formal or informal sport, or children's active play [7].

1.2. Pedestrian facilities and public open spaces

Access and linkages are the most important factors that make public spaces to be a great place [8]. A good public space network connects the different functions and public spaces of the city and invites people to walk. An attractive pedestrian network offers good climatic conditions and interesting things to look at, inviting people to walk. A comfortable pedestrian landscape has wide sidewalks of high-quality materials. Sidewalks should follow pedestrian desire lines and provide direct routes and direct access to buildings, open spaces and destinations. Sidewalks should be designed so that street furniture, trees, bicycle parking, signage, public transit stops, outdoor servings etc. do not block the area designated for walking. Streetscapes should be thoughtfully and artistically designed to draw more people to walk for both utility and pleasure [9].

Walking is a physical activity in public open spaces [10] [11]. Walking distance standards vary around the world. An individual's willingness to walk varies greatly depending on age, health, time availability, quality of surroundings, safety, climate, and many other factors. The majority of walking studies are for and about commuters. Most people are only willing to walk a quarter mile as part of a commute or approximate 400 meters in a single walking distance [12] [13]. Streets were once a place where people stopped for conversation. In the same time, pedestrian facilities are not only the ways for walking through but also, they are public open spaces. In addition, pedestrian facilities with streetscapes are design elements in public open spaces. These promote to attract people to use public open spaces [14]. They are easy to get to and get through; they are visible both from a distance and up close [14]. Moreover, walking is a green travel mode that is beneficial to the environment and the economy and can promote the health of campus users [15]. Previous research has mostly focused on using pedestrian facilities in campuses. Planners and designers are concerned with walking conditions to solve many problems (for example, global warming, health problems, energy consumption, air pollution, etc.). For instance, in Kasetsart University, walking is the third most frequent travel mode after private cars and public transport [16].

Pedestrian facilities in public open spaces are the basic tools of accessibility. Walking is the suitable type of connections for campuses because it makes no cost, promotes safety, leads to healthier life, and makes more communities. Paths are the elements that can help people to get the most sense of places [17].

2. Material and Methods

This study is a qualitative research by site surveying in four campuses which are located in Thailand and Hungary. Széchenyi István University, Gyor; Budapest University of Technology and Economics, Budapest; and University of Debrecen, Debrecen are three case studies in Hungary. Thammasat University is the one case study in Thailand. The methods of this study are divided into five steps leading to the result. They are: Subject specification, Literature review, Data collection, Data analysis, and Conclusion. The framework of the research is shown in Figure 1.

a(The study on the relationship between roles of public open spaces and its connections inside campus: The case study of the universities in Thailand and Hungary. There are two goals in this study as follows:

- To compare physical layouts of the campuses
- To compare relationship between roles and pedestrian facilities inside the campus

b(Literature review collects secondary data relating to concepts and theories concerning public open spaces and connections in campuses. The data come from many sources and features; they are editorial online papers, maps, pictures, spatial analysis from Geographic Information System)GIS(and Open Street Map)OSM(.

- Public open spaces, assessing the importance of public open spaces in the campus, character, pattern, size, shape, and type of public open spaces.
- Connections, consisting of roads for vehicles and pedestrian facilities in the campus and public open spaces, and the relationship between public spaces' layout and its pedestrian facilities.

c(Data are collected from site observations; the data are related to connections and convenience in public open spaces. Dependent variables are the layouts of the campuses and their public open spaces, surrounding, size, types of connections, and length of connections.

d(The analysis uses illustration by sketching and plotting zones, including analysis tools. They are Geographic Information System (GIS) and Open Street Map)OSM(.

- Illustration: This research applies this method for describing space from site observations. All primary data are managed by sketching and plotting on maps for easy clarification of the space.
- Spatial analysis: This research applies GIS (Geographic Information System) and Open Street Map)OSM(for spatial analyses to define types of connections. Furthermore, land use, roads for vehicles, and other characteristics of space are analysed.
- From section 3, we will get layouts of the campuses with spatial and accessibility details. They are location and surrounding, areas, the length of roads for vehicles and the length of pedestrian facilities.

e(Verification of this research is comparing the ratio of the length of connections per area in four campuses. They are the ratio of the length of road for vehicles per campus areas, the length of roads for vehicles per public open space areas, the length of pedestrian facilities per campus areas, and length of pedestrian facilities per public open space areas.

f(The conclusion of this research will be representing the relationship between roles and pedestrian facilities inside the campuses.
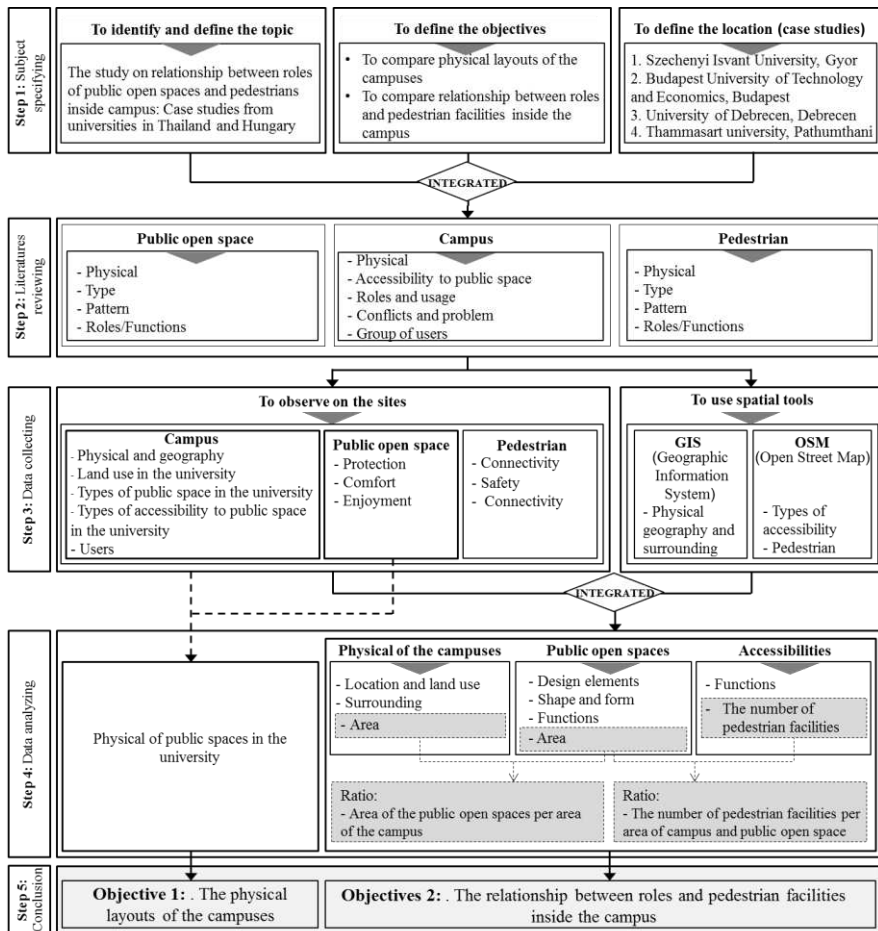
Figure 1. The framework of the study

3. Results and Discussion

3.1. Physical layouts of the campuses

The layouts of the campuses can be divided into two types by their location. In the first group, campuses were located in or near the city are Széchenyi István University and Budapest University of Technology and Economics. In the second group, the campuses were located far from the city with the cloistered environment like

Thammasat University and the University of Debrecen. Moreover, the campuses are different in size of the area and in the character of planning.

Referring to the following layouts of the campuses in Figure 2., it is visible that Széchenyi University and Budapest University of Technology and Economics are small and medium size of campuses. Both are located within a kilometre radius of the city. The campuses are surrounded by groups of residential and commercial land use with dense buildings. On the other hand, Thammasat University and the University of Debrecen are the two with the largest area, with big public open spaces. They are located far away from the city and surrounded by big open space. Both campuses have the character of a small town with facilities such as shops, banks, etc.
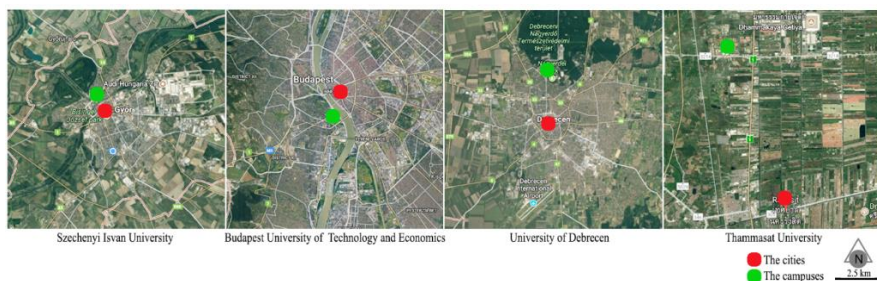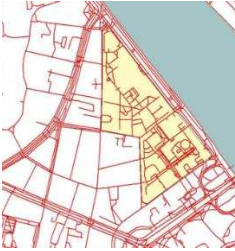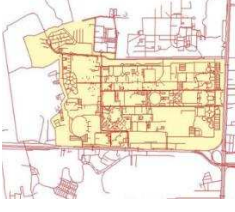

Figure 2. The layouts of the campuses

In terms of publicness and privacy, Széchenyi István University is the only one campus in the study that is a fully public space because it has no fences. Public open spaces inside the campus are always open. In addition, the campus connects to Mosoni Danube River on the West side. It is a big recreation park and beach where people can walk through from the public open space into the campus. On the other hand, Thammasat University, The University of Debrecen, and Budapest University of Technology and Economics are semi-public spaces or closed campuses. They are surrounded by fences and they are opened or closed by official hours. The main user of the campuses and their public open spaces are students and staff.

The layouts of the campuses containing the different connections and public open spaces are shown in Table 1.

The public open spaces in each campus have different physical outlines. They are distributed in many locations in campuses and they have also many shapes. For instance, there are big public open spaces connecting academic buildings, some are small and are surrounded by other places, or they are green areas as a greenbelt boundary. The differences of these public open spaces are various the identities or characters of the spaces.

Table 1. Layout and plans of the campuses

	Layouts	Connections	Public open spaces
Széchenyi István University Gyor			
Budapest University of Technology and Economics			
University of Debrecen			
Thammasat university (Rangsit campus), Pathumthani			

Public open spaces in Thammasat University and the University of Debrecen are big open spaces. They are located at the edge of the campus and they are separated from the building zones by roads for vehicles which is the main accessibility to the

public open space. Public open spaces in Széchenyi István University and Budapest University of Technology and Economics are located in the center of the campus areas. The public open spaces are surrounded by groups of buildings and also connected to the buildings by pedestrian facilities. The design elements are related with the use of these public open spaces. They are street furniture in public open spaces and landscape design for promoting comfort and convenience for users. There are trees, lawn, planting, colorful plants, facilities, natural views, pond, and so on. The main activities here are reading, sitting, standing around, chatting, social gathering, waiting, and passing by. The design elements in public open spaces and activities in each public open space are rather similar in the four campuses as shown in Table 2.

3.2. Relationship between roles and pedestrian facilities inside the campus

3.2.1. Pedestrian facilities in the campuses and their public open spaces

- Road for vehicles in the campuses
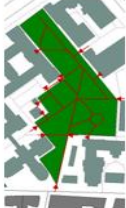
The lengths of the road for vehicles in Széchenyi István University, Budapest University of Technology and Economics, University of Debrecen, and Thammasat University are 1,518 m., 1,564 m., 10,996 m., and 44,609 m. respectively. Széchenyi István University and Budapest University of Technology and Economics have no roads for vehicles in their public open spaces. The lengths of the roads for vehicles in public open spaces in University of Debrecen and Thammasat University are 799 m. and 682 m. respectively.

Thammasat University has the highest ratio of the length of road for vehicles per square meter. It is 0.036)m./sq. m.(. Széchenyi István University and the University of Debrecen have approximate ratios. They are 0.017)m./sq. m.(and 0.015)m./sq. m.(respectively. Budapest University of Technology and Economics has the lowest ratio of the length of roads for vehicles per square meter. It is 0.005)m. /sq. m.(.

- Pedestrian facilities in the public open spaces

The lengths of pedestrian facilities in Széchenyi István University, Budapest University of Technology and Economics, University of Debrecen, and Thammasat University are 1,469 m., 5,141 m., 4,179 m., and 26,013 m. respectively. The lengths of pedestrian facilities in their public open spaces are 297 m., 667 m., 1,784 m., and 3,061 m. respectively.

Table 2. The environment and functions of the campuses

	Public Open Spaces	Surroundings and shape	Public open spaces and its connections	Design elements	Main activities
Széchenyi István university, Gyor				Trees Lawn Planting Colourful plants Facilities Natural views	Reading Sitting Standing around Chatting Social gathering Waiting Passing – by
Budapest University of Technology and Economics, Budapest				Trees Fountain Lawn Planting Colourful plants Facilities Natural views	Reading Sitting Standing around Chatting Enjoying scenery Social gathering Waiting Passing – by
University of Debrecen, Debrecen				Trees Fountain Lawn Planting Colourful plants Facilities Natural views	Reading Sitting Chatting Enjoying scenery Social gathering Waiting Passing – by
Thammasat university, Pathumthani				Trees Ponds Lawn Planting Colourful plants Natural views	Sitting Standing around Chatting Enjoying scenery Social gathering Waiting

- Ratio of length per area

The ratios of the length of roads for vehicles per campus areas of Széchenyi István University, Budapest University of Technology and Economics, University of Debrecen, and Thammasat University are 0.017 m., 0.005 m., 0.006 m., and 0.036 m. respectively.

The ratios of the length of roads for vehicles per public open space areas in University of Debrecen and Thammasat University are 0.004 m., and 0.003 m. respectively. Széchenyi István University and Budapest University of Technology and Economics have no this ratios because they have no roads for vehicles in their open spaces.

The ratios of the length of pedestrian facilities per campus areas are 0.016 m., 0.016 m., 0.006 m., and 0.021 m. respectively. And the ratios of the length of pedestrian facilities per public of open space areas are 0.057 m., and 0.053 m., 0.009 m., and 0.016 m. respectively (Table 3.).

3.2.2. The comparison of length and ratio of connections in the campuses.

Referring to Table 3, the comparison of spatial and accessibility details of the campuses are as follows:
- Széchenyi István University has the smallest areas, related both the campus and its public open space. Moreover, the campus has the shortest connections both road for vehicles and pedestrian facilities. On the other hand, the campus has the highest ratio of the length of pedestrian facilities in public open space per public open space area.
- Budapest University of Technology and Economics has the second smallest areas both the campus and its public open space. At the same time, the campus has the lowest ratio of the length of road for vehicles in the campus per campus area.
- University of Debrecen has the longest roads for vehicles in the public open spaces. Consequently, the campus has the highest ratio of the length of roads for vehicles in the public open space per public open space area. It has also the lowest ratio of pedestrian facilities per area related both the campus and the public open space area
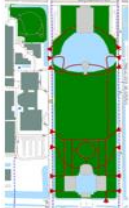- Thammasat University has the biggest area, related both the campus and its public open space. The campus has the longest roads for vehicles in the campus area. It has also the longest pedestrian facilities in the campus and in public open space areas. Moreover, the campus has the highest ratio of the length of roads for vehicles in the campus per campus area including the ratio of pedestrian facilities in the campus per campus area.

Table 3. Length and ratio of connections in the campuses

Campus	Area (sq. m.)		Length (m.)				Ratio (m. / sq. m.)			
			Road for vehicles		Pedestrian facilities					
	(A) Campus	(B) Public open space	(C) In the campus	(D) In the public open space	(E) In the campus	(F) In the public open space	(C)/(A)	(D)/(B)	(E)/(A)	(F)/(B)
Széchenyi István University, Győr	90,297*	5,255*	1,518*	0*	1,469*	297*	0.017	0*	0.016	0.057**
Budapest University of Technology and Economics	315,000	12,647	1,564	0*	5,141	667	0.005*	0*	0.016	0.053
University of Debrecen	739,232	189,480	10,996	779**	4,179	1,784	0.015	0.004**	0.006*	0.009*
Thammasat University, Pathumthani	1,225,235**	196,027**	44,609**	682	26,013**	3,061**	0.036**	0.003	0.021**	0.016

Note: X^* = the lowest number, X^{**} = the highest number

In conclusion, each public open space has pedestrian facilities longer than the road for vehicles. Széchenyi István University has the most pedestrian facilities in public open space. Following the forerunner, the ranking is: Budapest University of Technology and Economics, Thammasat University, and University of Debrecen. We can notice that the length of road for vehicles is related to the layouts of the campuses. Several campuses have long roads for vehicles, as seen in Thammasat University and University of Debrecen. Moreover, the character of building location is one of the factors that affects the length of roads for vehicles. If buildings or public open spaces in the campuses are connected with each other, the length of roads for vehicles will be small. On the other hand, the length of pedestrian facilities will be high. As shown in this study, Budapest University of Technology and Economics has many groups of buildings. They are located close to each other; some are even connected to each other. The lengths of roads for vehicles in the campus and in its public open space are shorter than in the other campuses. Therefore, the ratios of the roads for vehicles per the campus area and its public open space area are the lowest. They are only 0.005)m./sq. m.(and 0)m./sq. m.(respectively as shown in Table 3. Particularly, Széchenyi István University has only pedestrian facilities in its public open space. In addition, Széchenyi István University has the highest ratio of pedestrian facilities in public open space per public open space area. It is 0.057)m. /sq. m.(as shown in Table 3.

It was found that the different lengths of pedestrian facilities are related to the layout of the campuses and the functions of their public open spaces. Pedestrian facilities are the main connections to public open spaces. The spatial arrangement of pedestrian facilities is influenced by the following three factors (Figure 3).

a) The size of the campus and its public open space: Pedestrian facilities are good for connecting buildings and public open spaces in acceptable distance for humans. Because a single walking distance standard for all situations is 400 meters, thus the smaller the areas, the closer the distance the pedestrians are using. On the other hand, the bigger the areas, the longer are the distances. In this case, the road for vehicles is important to connect buildings and public open spaces.

b) Surrounding of the campus and its public open space: Design and planning zones, groups of buildings, and public open spaces in the surrounding are affecting the types of connections. If the surrounding it built-in, pedestrian facilities will be created. Furthermore, a short distance between buildings and public open spaces is attracting people to walk because of building shadow.

c) Design elements: All four public open spaces in the campuses have elements of landscape designs. They promote safety, comfort, and convenience to users for using the spaces including supporting the aesthetic in public open spaces.
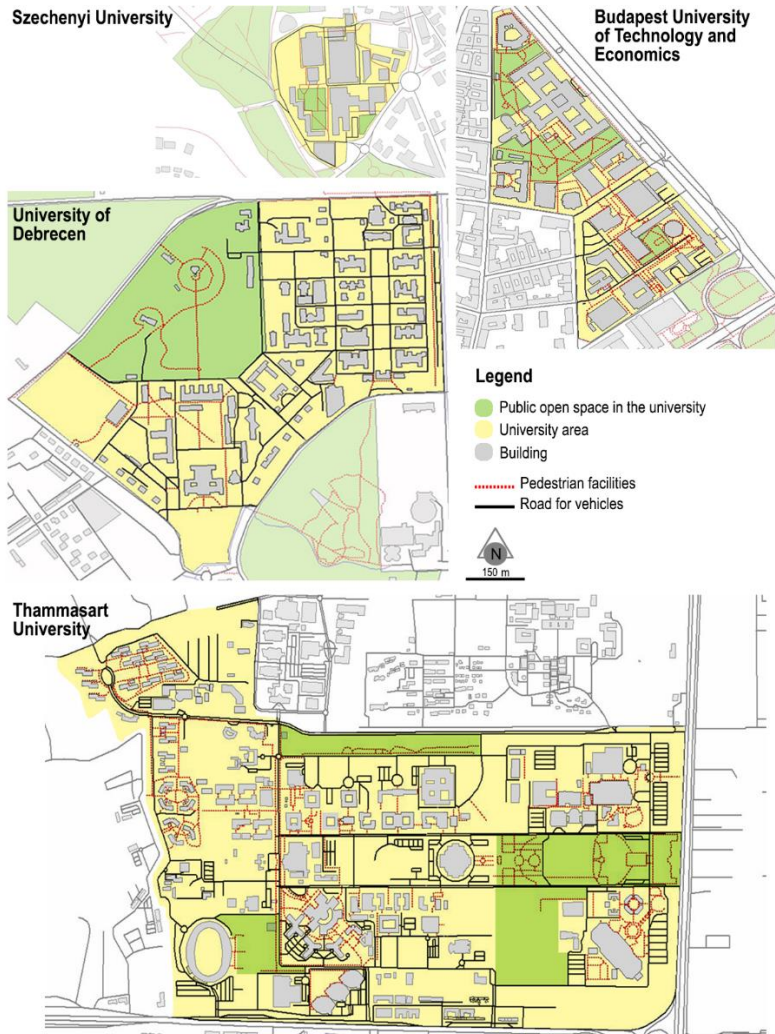
Figure 3. Land use and connections in the campuses

4. Conclusions

Campuses are important places to students and staff, including the community around the campuses. Consequently, layout and planning of campuses should match with the context and the surrounding. The open space also creates a pedestrian precinct that is connected by circulation pathways through which the students and staff pass in their movement from parking, walkways, and buildings. Pedestrian facilities are the main means of mobility to public open spaces in the campuses. These facilities are related to the different layouts of the campuses including the size of the campus and its public open space, the surrounding the campus and its public open space, and its design elements.

This study only used site surveying and spatial analysis data from Geographic Information System)GIS(and Open Street Map)OSM(. For future study, questionnaires will be used for collecting information about user's behaviors and preferences. The relationship between the layout and the usage will add more value to the study.

Acknowledgement

References

[1] H. Arendt, The Public and the Private Realm, in: The Human Condition, University of Chicago Press, Chicago, 1998, pp. 182-230.

[2] A. Madanipour, Whose Public Space? Routledge. New York, 2010.

[3] J. Walljasper, Big Plans on Campus (2009) [cited 2020-01-27].
     URL *https://www.pps.org/reference/campusbulletin/*

[4] P.K. Baran, W.R. Smith et al. Park use among youth and adults: examination of individual, social, and urban form factors. Environment and Behavior 46 (6) (2013) pp. 768–800.
     doi: *https://doi.org/10.1177/0013916512470134*

[5] A.T. Kaczynski, K.A. Henderson. Parks and recreation settings and active living: a review of associations with physical activity function and intensity,

Journal of Physical Activity and Health 5 (4) (2008) pp. 619–632.
doi: *https://doi.org/10.1123/jpah.5.4.619*

[6] C. Holland, A. Clark et al.: Social interactions in urban public places. The Open University, Policy Press, Bristol, 2007. [cited 2020-01-27].
URL*https://www.jrf.org.uk/sites/default/files/jrf/migrated/files/2017-interactions-public-places.pdf*

[7] M.J. Koohsari, S. Mavoa et al. Public open space, physical activity, urban design and public health: Concepts, methods and research agenda. Health & Place 33 (2015) 75–82.
doi: *https://doi.org/10.1016/j.healthplace.2015.02.009*

[8] Project for Public Spaces and Metropolitan Planning Council. A Guide to Neighborhood Placemaking in Chicago, Project for Public Spaces, New York, 2008. [cited 2020-01-27].
URL *http://www.placemakingchicago.com/cmsfiles/placemaking_guide.pdf*

[9] Gehl Graphic Library. Public Space & Pedestrian Realm. A. Connectivity – The Public Space Network, 2011. [cited 2020-01-27].
URL *http://www.bettermarketstreetsf.org/docs/BMS_P2-1_BestPractices_12072011.pdf*

[10] J. Schipperijn, U.K. Stigsdotter et al. Influences on the use of urban green space—A case study in Odense, Denmark, Urban Forestry and Urban Greening 9 (1) (2010) pp. 25–32.
doi *https://doi.org/10.1016/j.ufug.2009.09.002*

[11] T. Sugiyama, J. Francis et al. Associations between recreational walking and attractiveness, size, and proximity of neighborhood open spaces. American Journal of Public Health, 100 (9) (2010) pp. 1752-1757.
doi *https://doi.org/10.2105/AJPH.2009.182006*

[12] T. Morar, L. Bertolini, Planning for Pedestrians: A Way Out of Traffic Congestion, Procedia - Social and Behavioral Sciences 81 (2013) pp. 600-608.
doi: *https://doi.org/10.1016/j.sbspro.2013.06.483*

[13] J. Walker, Human Transit. basics: walking distance to transit (2011) [cited 2020-01-27].
URL *http://humantransit.org/2011/04/basics-walking-distance-to-transit.html*

[14] W.H. Whyte, Streets as Places: How Transportation Can Create a Sense of Community, Project for Public Spaces (2014) [cited 2020-01-27].
URL *www.pps.org/reference/streets-as-places-how-transportation-can-create-a-sense-of-community*

[15] Z. Asadi-Shekari, M. Moeinaddini, M. Zaly Shah, A pedestrian level of service method for evaluating and promoting walking facilities on campus streets, Land Use Policy 38 (2014) pp. 175–193.
doi *https://doi.org/10.1016/j.landusepol.2013.11.007*

[16] R. Panitat, The appropriate walkway towards sustainable transportation in the university community: A case study of Kasetsart University, 16th Annual International Sustainable Development Research Conference, Bangkhen Campus, Hong Kong, China, 30 May – 1 June 2010.

[17] K. Lynch, The Image of the City, The M.I.T. press, Cambridge, 1990.

FEM Modelling Possibilities of Glued Insulated Rail Joints for CWR Tracks

A. Németh[1], Z. Major[1], Sz. Fischer[1,*]

**[1]Széchenyi István University, Department of Transport Infrastructure and
Water Resources Engineering
Egyetem tér 1., 9026 Győr, Hungary
e-mail: fischersz@sze.hu**

Abstract: In this paper the authors detail the possibilities of modelling of finite element method (FEM) of glued insulated rail joints which are applied in railway tracks with continuously welded rails (CWR). A lot of laboratory tests (static and dynamic 3-point bending tests, axial pulling tests) were executed on glued insulated rail joints, the specimens were related to three different rail profiles applied in Hungary: MÁV 48.5; 54E1 (UIC54), 60E1 (UIC60), respectively. The static bending tests with many bay length values were conducted, before and after dynamic (fatigue) tests. 2-D beam models were made in FEM software using semi-rigid hinge as the simplified connection of fishplated glued insulated rail joint. The FEM models were calibrated and then validated with the static vertical displacement values in the middle-bay position measured in laboratory. The model validation was conducted with two methods.

Keywords: glued insulated rail joint; laboratory test; finite element modelling; calibration; validation

1. Introduction and literature review

The connection of rails applying fishplated rail joints with horizontal axis bolts is one of the weakest points of construction of railway tracks, mainly in CWR tracks, as well as in case of small horizontal curves and turnouts. In the traditional set-up there are two fishplates (i.e. a pair of fishplates) for joining of the adjacent rail ends with four or six steel bolts. The reason of this structure is to connect rail ends avoiding vertical and horizontal steps in the middle of rail joint (i.e. in the zone of

endpost element). This kind of set-up ensures the smooth running and guiding edges and surfaces of the rails at rail joints to be able to reduce the evolving dynamic forces due to passing wheels. This is one of the base requirements of the railway tracks. The gaps between rail ends, the inadequate configuration of the horizontal and vertical profile of joined rail ends brake the continuity of railway tracks. In CWR tracks glued insulated rail joints (GIRJs) have to be applied because of the railway signalling and safety control, as well as the high axial (mainly thermal) forces evolved in the rails. It has to be mentioned that in normal railway tracks with traditional fishplated rail joints (without glue material, i.e. IRJs) are used with or without insulation according to railway signalling and safety control systems.

In international literature there are a lot of articles and research reports that are dealing with fishplated rail joints (traditional set-up with and without insulation, as well as special insulated ones with glue material, i.e. glued insulated rail joints). Regarding to fishplated glued insulated rail joints the most problems are the false railway control signs due to rail ends failures which resulting the railway capacity restriction. Other problems are for example the implementation of glue material, endposts, rail ends and wear of rail profile inner corner and plastic deformation.

According to this paper the authors introduce the relevant research results of mainly FEM modelling, as well as some other interested literature related to fishplated rail joints.

There are some interesting results from the international literature review:

- in generally the rail joints' failure is connecting to decreased moment of inertia of the pair of fishplates (compared to applied rail section) [1], and enlarged stress values in the head of the rail that can result plastic deformation, lipping in the rail steel material [2],

- the maintenance cost of rail joints is significant high, it is very problematic issue to avoid insulated rail joints from railway tracks (mainly CWR tracks) [1],

- it is very serious to select suitable type of glue for glued insulated rail joints [3] [4]. It is important and significant issue specially related to the material and thickness of endpost elements [5] [6] [7] [8]. The significance of this issue is also detailed in papers [9] [10] [11]. In these publications the authors stated the most appropriate type of endpost elements to be applied in fishplated rail joints,

- modified geometry in the head of rail section (longitudinal section, i.e. arch shape) is able to provide lower arising stresses and expand the life-time of fishplated rail joints [12],

- lipping phenomena in the rail head near the endpost is able to be set back by better rail steel grade or altered-treated steel types applied in rail head [5] [13] [14],

- external reinforcement methodologies can provide increased bending stiffness of rail joints assembled with fishplates [1],

- the application of non-perpendicular (i.e. for example 30° and 45°, in other words: inclined) rail joints is able to reduce vertical deformation, noise and vibration compared to normal ones (i.e. perpendicular joint types) [12],

- it has to be marked that inclined fishplated rail joints aren't suitable (i.e. they aren't more appropriate than square ones), it is based on practice of railway operators [15],

- significance of glue arrangement (together with the volume of glue between fishplates and rail web) [16],

- the arising stress-strain state of the rail joint elements is affected by the support geometry types [3] [17] [18],

- significant stresses can be evolved due to wheel-rail contact in the rail head, as well as in the fishplated rail joint's elements that can lead to plastic deformation and early failures [19] [20] [21] [22],

- rail joints are able to result supplementary (extra) dynamic effect that can issue with much more rapid deterioration process [23] [24] [25] [26].

- Related to dynamic effect at turnout frogs a research group dealt at TU Dresden [27] [28] [29] [30]. They detailed that adequate geometry and well-chosen rail (and/or rail head) steel materials are suitable to reduce dynamic effect during wheel passing. It can increase the lifetime of the turnout frog and frog nose that results in reduction of life cycle costs (LCC). In the paper [31] they applied special multi-fractal analysis. This area is highly interesting related to fishplated rail joints because there are many connection points between these researches.

- At Railway University of Dnipropetrovsk there is a team which researched mainly the evolved stress-strain state of the whole railway track with very sophisticated methods [32] [33] [34] [35]. In the paper [36] they investigated the railway track representation in mathematical model of vehicles movement. Irregular vehicle movements are a key issue related to arising 'extra' stresses in the elements of railway track, also in IRJs and GIRJs.

After the authors have finished laboratory and field tests on glued insulated rail joints with glass-fibre reinforced and steel fishplates the necessity of applicability of polymer-composite fishplated glued insulated rail joints (synonym of glued insulated rail joints with glass-fibre reinforced fishplates) based on FEM modelling. In their papers [37] [38] [39], they dealt with laboratory tests of IRJs and GIRJs. In publications [40] [41] [42] there are investigations related to field tests. A lot of laboratory tests (static and dynamic 3-point bending tests, axial pulling tests) were executed on glued insulated rail joints, the specimens were related to three different rail profiles applied in Hungary: MÁV 48.5; 54E1 (UIC54), 60E1 (UIC60). The static bending tests with many bay length values were conducted, before and after dynamic (fatigue) tests. 2-D beam models were made in FEM software using semi-rigid hinge as the simplified connection of fishplated glued insulated rail joint. The FEM models were calibrated and then validated with the static vertical displacement values in the middle-bay position measured in laboratory. The model validation was conducted with two methods, detailed in the following sections.

The advantage of FEM modelling can be economic aspects. The calibrated and validated FEM models can be applied to be able to assume the behaviour of fishplated rail joints (with the consideration of used parameters). It is useful for saving time and money (i.e. resources) because the expensive and time consuming laboratory tests are not needed to execute every time. It has to be mentioned that our FEM models are adequate to approximate the mechanical behaviour (without failure) of glued insulated rail joints with glass-fibre reinforced fishplates with the applied one kind of glue material. In case of more complex investigation is needed, supplementary laboratory tests have to be conducted, i.e. with more types of glue materials, more rail profiles, more types of fishplates, etc. These tests can be executed in the future that is a real plan of the authors.

2. Methods

The following methods were applied in the research related to this paper:

- laboratory tests,
- FEM modelling,
- mathematical statistics and regression calculations,
- calibration,
- validation.

Laboratory tests of the authors are detailed in [37] [38] [49] literatures. A lot of laboratory tests were performed, not only those the authors mentioned in this article. Most of them were static and dynamic 3-point bending tests until breakage or without breakage (in the elastic material behaviour range).

FEM modelling was applied with simple 2-D models in Axis VM software.

Mathematical statistics 'tools' were used to determine simple mathematic parameters, values (i.e. average, standard deviation, etc.) and to define their adequacy. Regression calculations were applied to define and compose adequate and applicable mathematical regression functions to be able to calculate values for internal points from the trends or to be able to approximate the external points (extrapolation).

For the FEM models calibration and validation steps had to be done to achieve appropriate models that can be used for easy and quick calculations and avoid the performance of expensive and time-consuming laboratory tests.

Again, the mathematical regression calculations were suitable to be able to determine special equations with that the FEM calculations can be neglected in determined value (parameter) interval(s).

3. Laboratory tests

In this chapter the authors' own made laboratory tests are shortly introduced. These tests were conducted on three different rail profiles: MÁV 48.5, 54E1 (UIC54) and 60E1 (UIC60), which were assembled by MÁV-THERMIT Ltd. These specimens were not the part of research and development made for MÁV (Hungarian Railways) between 2015 and 2017. These specimens are very new assembled ones, especially for supplementary tests with more detailed measurements.

The details of laboratory tests' parameters can be found in Table 1. [39].

Table 1. Calculated and applied bending moment values for GIRJs with three different rail profiles

Rail profile	Bending moment [kNm]
60E1	42.63
54E1	40.85
MÁV 48.5	34.71

The values of maximum concentrated vertical loads can be calculated from the bending moment for each type of glued insulated rail joint and for each bay length value (see eq. (1)).

$$F_{max} = \frac{4 \cdot M_{max}}{L},$$
(1)

where

- F_{max} is the value of maximum concentrated vertical load in kN unit,

- M_{max} is the value of maximum bending moment in kNm unit from Table 1.,

- L is the bay length (support bay length) of the specimen in m unit.

The relevant laboratory tests on glass-fibre reinforced fishplated glued insulated rail joints are the followings related to the base of FEM modelling (the loading assembly was symmetric):

- static 3-point bending tests before fatigue tests (BF) – on 13 different bay lengths, between 900 and 1490 mm with 50 mm steps (see Fig. 1.),
- dynamic fatigue tests with steps of 0.5 million loading cycles on 1200 mm bay length,
- after every 0.5 million loading cycles there were static 3-point bending tests (without failure) up to 3.5 million loading cycles on the same bay length as BF tests (AF) – it has to be mentioned that the measurements after 3.0 million cycles have to be neglected because of inadequate test set-up,
- supplementary static 3-point bending tests after 3.5 million loading cycles (AF) – on 6 different bay lengths, between 600 and 850 mm with 50 mm steps.

Figure 1.   Assemblage for loading the glued insulated rail joint

From each measurement (static bending tests BF and AF) the authors recorded the vertical loading force vs. vertical displacement of the middle bay point of the rail joints graphs. (It has to be mentioned that at more points were the vertical displacement values measured and recorded, but in this research they are not considered.)

Because of the significant quantity of measured data, the authors don't publish all of them. They applied these data for the finite element modelling, in this way only the obtained new parameters will be published based on the laboratory tests.

4. Finite element modelling

4.1. Short description of FEM modelling with Axis VM software

In the following paragraph the authors shortly describe the main characteristics of Axis VM software [43].

It can be applied for the static, vibration, and buckling analysis of structures. At every step of the modelling process, graphical verification of the user's progress is sent. Multilevel undo/redo command and on-line help is available. Static, vibration, and buckling analysis are ensured.

Deformed and undeformed shape display, diagram, iso-line/surface plots, animation, customizable tabular reports are possible 'outputs' of the analyses.

Axis VM software grants special visualization tools that let the user fast explain the results, and numerical tools to search, report, and execute further calculations using those results. The results are able to be applied to illustrate the deformed or animated shape of the user's geometry or the isoline/surface plots. Axis VM can linearly compose or envelope the results.

Reporting is always part of the analysis, and a graphical user interface enhances the process and simplifies the effort.

4.2. Parameters of FEM models

Only one data pair has to be registered and used for FEM modelling from the laboratory tests from each measurement. It is the maximal vertical displacement values of middle bay point due to the maximal loading force values (they are calculated from the considered bending moment and bay length values [39].

The authors had to collect all of these data pairs to be able to apply them in FEM models.

The simplified FEM model is a 2-D model, the characteristics are the following:

- geometry:
    - elements: simple line (beam) elements, the geometry is the same as during laboratory tests,
    - supports: two simple hinge supports,
    - material: S235 type steel,
    - cross-section: exact rail profiles from CAD drawings,
    - semi-rigid hinge: it substitutes the fishplated joint and its mechanical behaviour,

- loads:
    - concentrated vertical forces as calculated from Zimmermann-Eisenmann method (see Table 1. and Eq. (1)) [37] [38] [39],

- calculation method:
    - simple static calculation with elastic material method,

- results:
    - elastic deformation lines from them the vertical displacement values of middle bay point are relevant.

4.3. Calibration and validation of FEM models

The FEM models have to be calibrated before their application. It means that there should be more laboratory tests, measurements whose data have to be used for model calibration.

The authors' FEM models are simplified models. It means that only one parameter has to be set during calibration: the hinge characteristic for rotation in the plane of the beam. The symbol of this 'rigidity' is α_{srh} (srh means semi-rigid hinge), the unit is kNm/rad. After calculation in Axis VM software there will be elastic deformation line of the beam, the vertical displacement can be determined for each point of the beam. The vertical deformation value of the middle bay point should be the same as in the laboratory tests for each cases (each bay length, each rail profile, etc.) The α_{srh} parameter has to set (i.e. calibrated) with iteration until the before mentioned displacement value is the same in FEM modelling as from laboratory tests. With this procedure 13…16 α_{srh} values can be calculated for each loading status (i.e. for BF and every AF step). For one kind of rail profile there are 7 loading status:

- BF, i.e. 0 loading cycle (BF),

- AF related to 0.5 million loading cycles (AF(0.5M)),

- AF related to 1.0 million loading cycles (AF(1M)),

- AF related to 1.5 million loading cycles (AF(1.5M)),

- AF related to 2.0 million loading cycles (AF(2M)),

- AF related to 2.5 million loading cycles (AF(2.5M)),

- AF related to 3.5 million loading cycles (AF(3.5M)).

Figure 2. shows an example about the FEM model in Axis VM software.
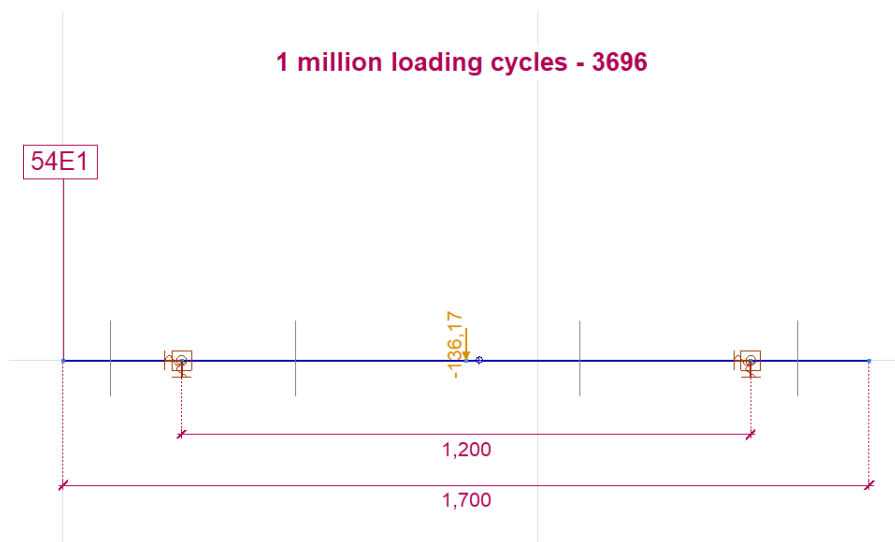
Figure 2.   Schematic, semi-calibrated FEM model of glued insulated rail joint with 54E1 rail profile (L=1200 mm, AF(1M), α_{srh}=3696 kNm/rad)

The model validation was conducted with two methods:

- **Case I.**, calibration with data related to static tests up to 2.5 million fatigue cycle and validation of the measurements related to static tests after 3.5 million loading cycle; as well as

- **Case II.**, calibration with data related to static tests with 3.5 million fatigue cycle in the interval of support bays between 1000 and 1490 mm and validation of the measurements related to static tests in the interval of support bays between 600 and 950 mm.

In Tables 2-4 the values of α_{srh} parameter of investigated glued insulated rail joints are represented. These values are calculated from Axis VM software, but it should be mentioned that these are based on the laboratory test results, the FEM calculations

were executed related to these vertical deflection values in the middle of the support bay. It can be seen that the standard deviation values vary approx. between 3% and 12%, these relatively high values are because of the quality of the polymer composite fishplates, glue material, assemblage, etc. It should be mentioned that these standard deviations influence the calibration, validation and the final accuracy of built FEM model.

Table 2. Values of α_{srh} parameter of investigated glued insulated rail joints (60E1 rail profile) calculated by Axis VM software

No. of loading cycles/values	BF	AF(0.5M)	AF(1M)	AF(1.5M)	AF(2M)	AF(2.5M)	AF(3.5M)
min.	6950	6700	6640	6390	6310	6170	5170
max.	10800	8320	7770	7600	7550	7470	7150
average	7978.462	7464.615	7320.769	7163.846	7096.154	6865.385	6271.053
standard deviation	989.283	420.290	347.886	356.313	367.436	487.675	617.278
standard deviation/ average	12.40%	5.63%	4.75%	4.97%	5.18%	7.10%	9.84%

Table 3. Values of α_{srh} parameter of investigated glued insulated rail joints (54E1 rail profile) calculated by Axis VM software

No. of loading cycles/values	BF	AF(0.5M)	AF(1M)	AF(1.5M)	AF(2M)	AF(2.5M)	AF(3.5M)
min.	4746	3740	3447	3426	3300	3267	3095
max.	5512	4133	3854	3780	3674	3545	3504
average	5162.385	3971.308	3683.538	3592.077	3459.308	3386.846	3236
standard deviation	261.943	120.767	121.904	106.471	124.330	98.333	125.813
standard deviation/ average	5.07%	3.04%	3.31%	2.96%	3.59%	2.90%	3.89%

Table 4. Values of α_{srh} parameter of investigated glued insulated rail joints (MÁV 48.5 rail profile) calculated by Axis VM software

No. of loading cycles/values	BF	AF(0.5M)	AF(1M)	AF(1.5M)	AF(2M)	AF(2.5M)	AF(3.5M)
min.	4845	4376	4259	4220	3968	3667	3250
max.	6035	5035	4898	4693	4470	4457	3977

average	5473.154	4737	4481.615	4392	4201.154	4040.769	3623.368
standard deviation	356.348	207.150	180.519	130.103	155.162	231.602	167.628
standard deviation/ average	6.51%	4.37%	4.03%	2.96%	3.69%	5.73%	4.63%

In Figure 3. the trends of changing of average α_{srh} parameter as a function of number of loading cycles in the whole measured interval are shown. It can be seen that during the first 500,000 loading cycles there are a relatively rapid decrease of α_{srh} (i.e. rapid deterioration of glued insulated rail joint) related to all of the investigated rail joints, but after 500,000th loading cycle the trend changes to approx. linear, as illustrated in Figures 3-4. It is very interested fact that specimen assembled with 54E1 rail profile and related polymer composite fishplate is a little bit worse than the specimen with MÁV 48.5 rail profile, but the trend is consequent. It can be due to the mentioned reasons.
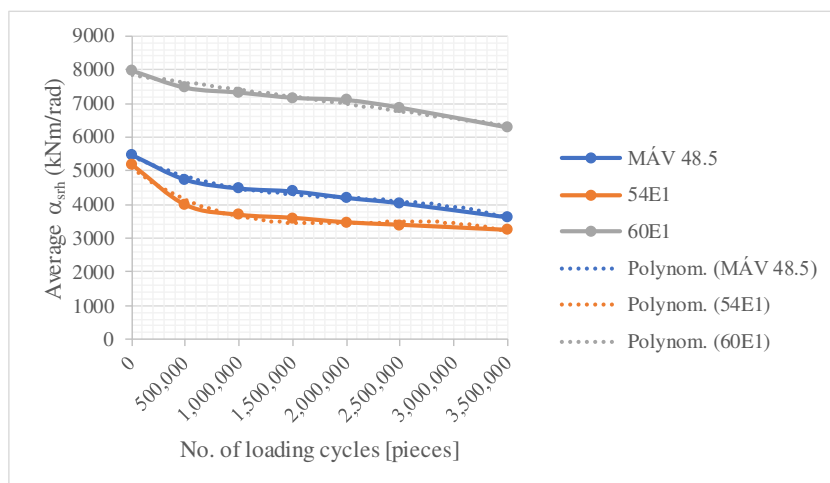
Figure 3.   Trends of changing of average α_{srh} parameter as a function of number of loading cycles in the whole measured interval
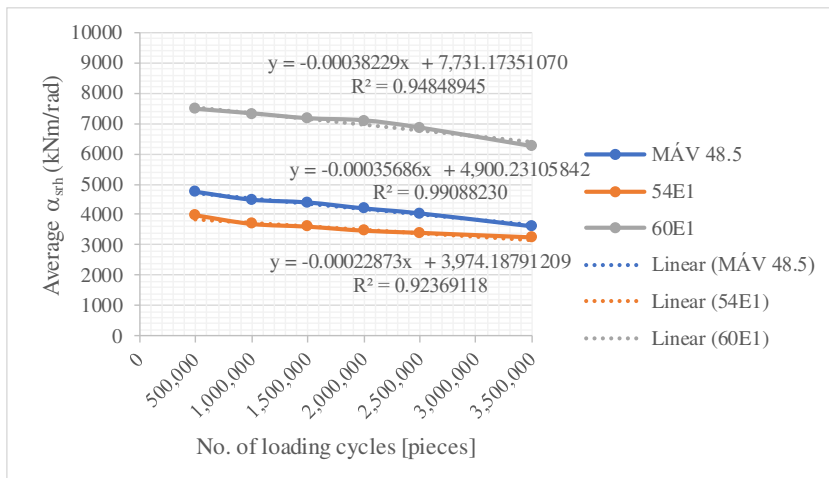
Figure 4. *Trends of changing of average α_{srh} parameter as a function of number of loading cycles between 500,000 and 3.5 million cycles*

In Figure 5. the linear regression functions can be seen that are applied for calibration *Case I.* (as earlier mentioned).
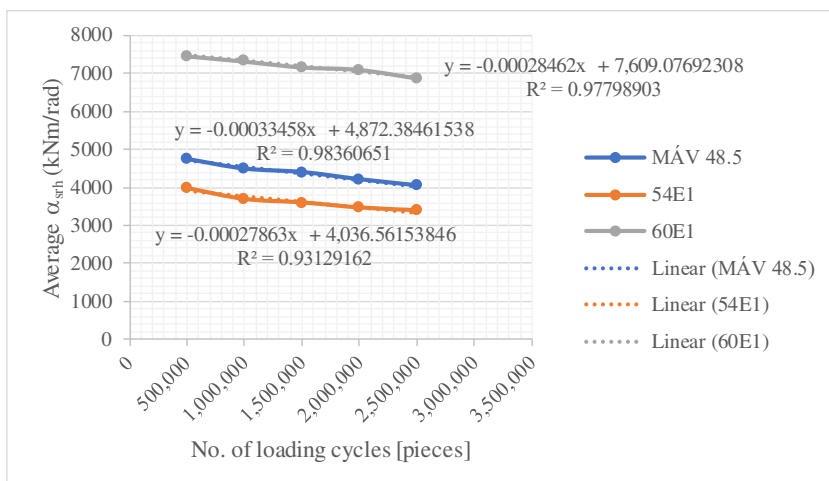
Figure 5. *Trends of changing of average α_{srh} parameter as a function of number of loading cycles between 500,000 and 2.5 million cycles*

The values of calculated α_{srh} parameters for 3.5 million loading cycles (with extrapolation) are represented in Table 5.

Table 5. The values of calculated α_{srh} parameters for 3.5 million loading cycles (with extrapolation)

Rail profile	Calculated α_{srh} [kNm/rad]	Deviation from the measured value
60E1	6612.907	5.45%
54E1	3061.357	−5.40%
MÁV 48.5	3701.355	2.15%

In case the semi rigid hinge of the beam models is set to values in Table 5. The deviations from the measured values in reality were calculated and shown in Table 6. This the result of calibration and validation of *Case I*.

Table 6. The values of calculated α_{srh} parameters for 3.5 million loading cycles

Rail profiles/ characteristics of deviation values	60E1	54E1	MÁV 48.5
min.	−18.44%	0.87%	−10.44%
max.	5.54%	12.15%	4.89%
average	−4.39%	4.59%	−1.92%
standard deviation	7.29%	3.31%	3.63%

The higher deviation values in Table 6. (e.g. −18.44%, 12.15%) are related to the small bay length values (600…850 mm).

In *Case II.* the results (calibration and validation) are obtained published in Tables 7-8.

Table 7. The values of calculated α_{srh} parameters for 600…950 mm bay length values (with statistical calculation)

Rail profiles/ values	60E1	54E1	MÁV 48.5
min.	5960	3095	3542
max.	7150	3374	3977
average	6655.455	3233.636	3717.182
standard deviation	459.921	109.318	124.795
standard deviation/ average	6.91%	3.38%	3.36%

Table 8. The deviations from the measured values in reality (validation related to Case II., the base of comparison is the vertical deflection values)

Rail profiles/ characteristics of deviation values	60E1	54E1	MÁV 48.5
min.	–18.89%	–3.25%	–10.76%
max.	–4.42%	7.02%	–1.48%
average	–11.20%	0.11%	–4.85%
standard deviation	4.66%	4.03%	3.01%

5. Results

In Chapter 4. the authors showed the results of the calibration and validation processes. The obtained broad interval of the accuracy (up to approx. 20%) is (or can be) because of the the earlier mentioned reasons, i.e. the quality of the polymer composite fishplates, glue material, assemblage, etc.

In the future the authors recommend to apply the average values of the Tables 2-4 for running FEM models.

Next to the calibration and validation results there are some interesting supplementary results from the FEM modelling. A lot of calculations were

performed in Axis VM software with the built model of glued insulated rail joints. The α_{srh} parameter was changed between 100 and 10^6 kNm/rad values.

In Figures 6-14. the authors introduce charts related to vertical displacement as a function of bay length for different α_{srh}. In these figure some of them are shown between 10^3 and 10^6 kNm/rad. It can be stated that the calculated points can be approximated by power regression functions. One of the lines of a figure is the same in the following figure related to each rail profile because in this way the difference can be considered more accurate.
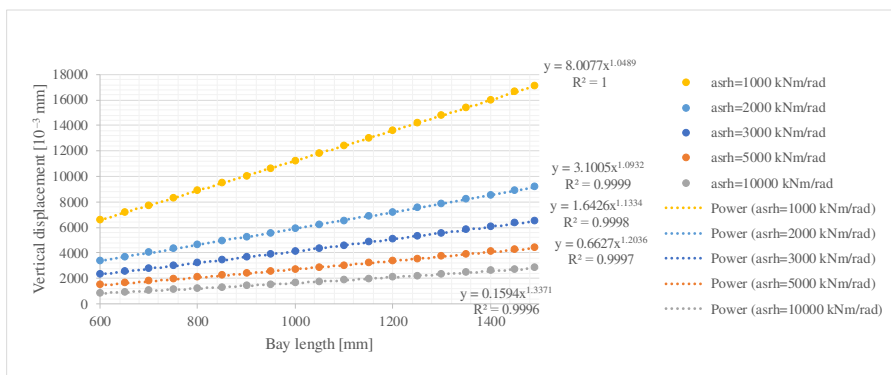
Figure 6.   Vertical displacement as a function of bay length related to different α_{srh} values (between 1000 and 10000) in case of fishplated rail joint with 60E1 rail profile
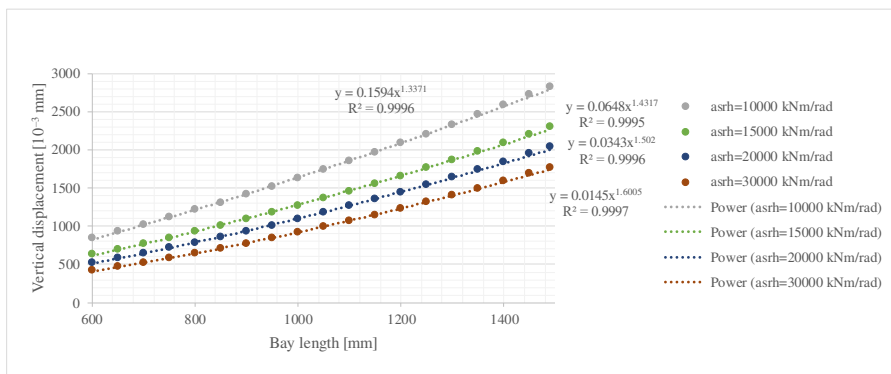
Figure 7.   Vertical displacement as a function of bay length related to different α_{srh} values (between 10000 and 30000) in case of fishplated rail joint with 60E1 rail profile
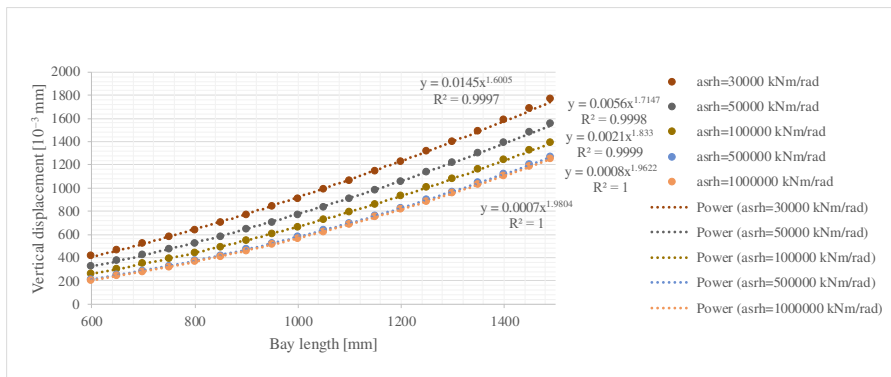
Figure 8. Vertical displacement as a function of bay length related to different α_{srh} values (between 30000 and 1000000) in case of fishplated rail joint with 60E1 rail profile
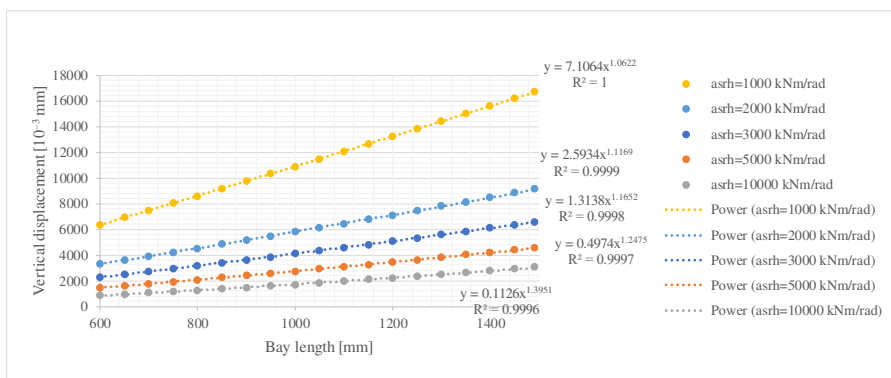
Figure 9. Vertical displacement as a function of bay length related to different α_{srh} values (between 1000 and 10000) in case of fishplated rail joint with 54E1 rail profile
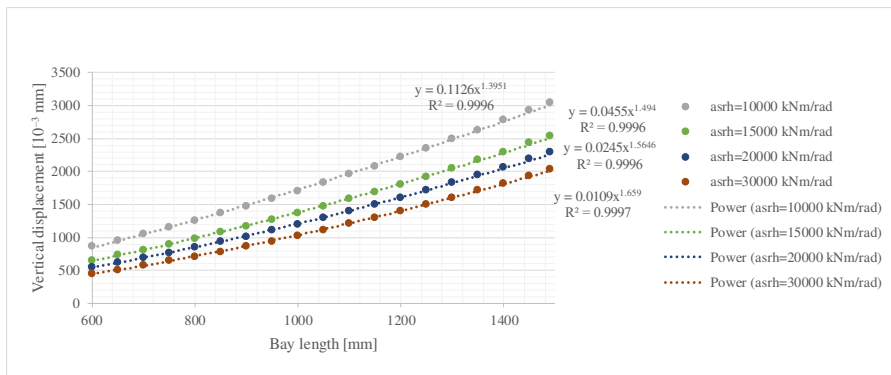
Figure 10.   Vertical displacement as a function of bay length related to different α_{srh} values (between 10000 and 30000) in case of fishplated rail joint with 54E1 rail profile
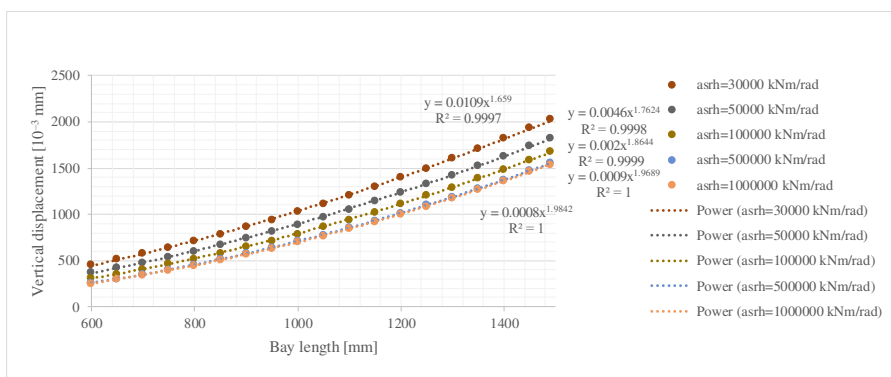
Figure 11.   Vertical displacement as a function of bay length related to different α_{srh} values (between 30000 and 1000000) in case of fishplated rail joint with 54E1 rail profile
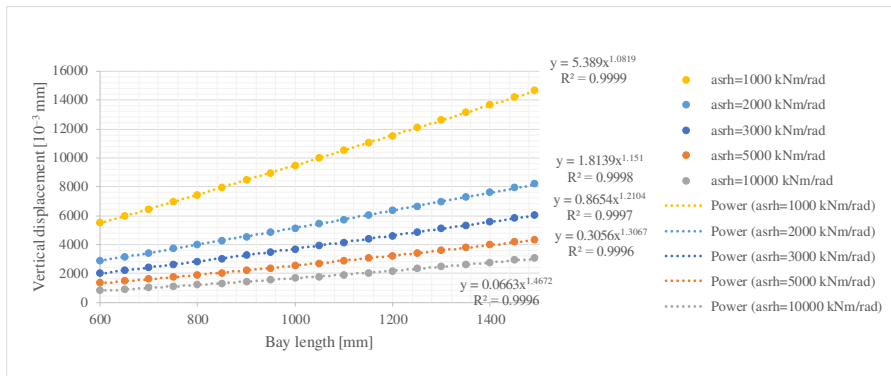
Figure 12.   *Vertical displacement as a function of bay length related to different α_{srh} values (between 1000 and 10000) in case of fishplated rail joint with MÁV 48.5 rail profile*
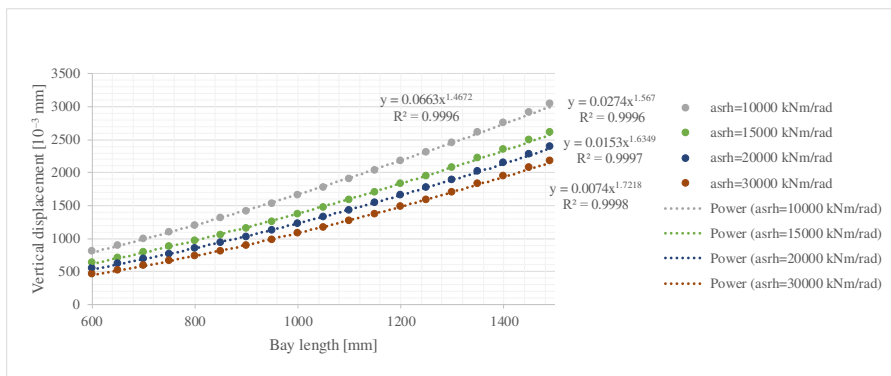
Figure 13.   *Vertical displacement as a function of bay length related to different α_{srh} values (between 10000 and 30000) in case of fishplated rail joint with MÁV 48.5 rail profile*
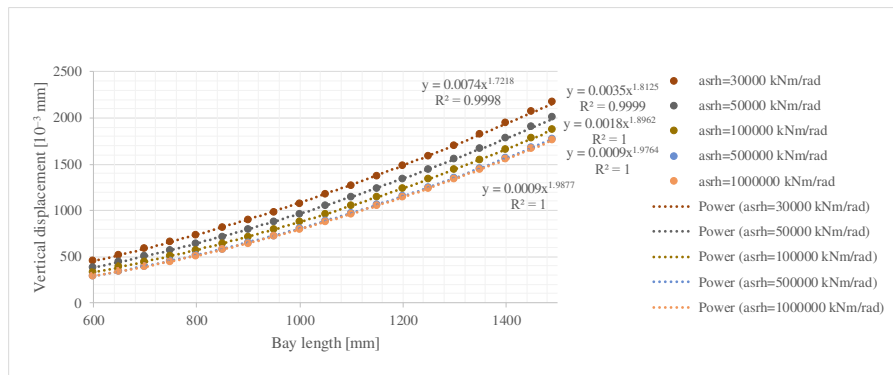
Figure 14. *Vertical displacement as a function of bay length related to different α_{srh} values (between 30000 and 1000000) in case of fishplated rail joint with MÁV 48.5 rail profile*

To be able to calculate much faster the α_{srh} parameters from vertical displacement values, as well as vice versa the authors determined definite regression functions for the range of α_{srh} from 100 to 30000. In the interval between 30000 and 10^6 the determined regression functions are not enough accurate.

In Figure 15. there is a raw regression function related to fishplated rail joint with 60E1 rail profile and L=600 mm bay length for the whole $100…10^6$ kNm/rad interval.
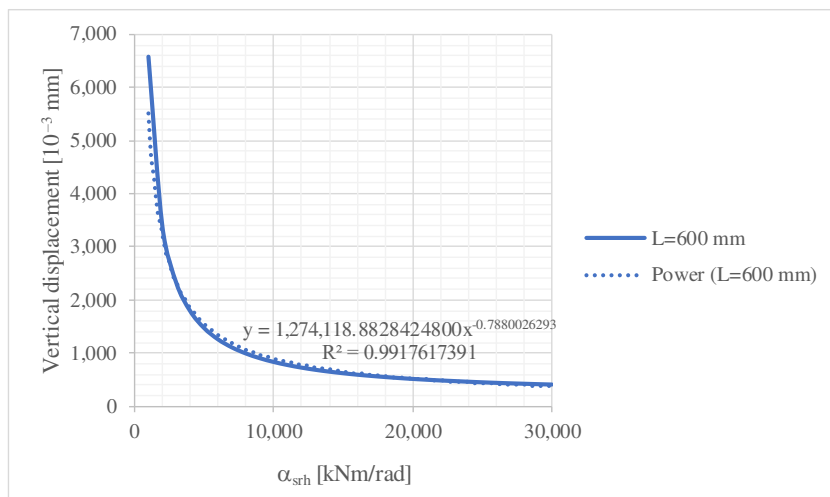
Figure 15.   Vertical displacement as a function of α_{srh} in case of fishplated rail joint with 60E1 rail profile and L=600 mm bay length

In Figure 15. the determined power regression is not adequate for calculation vertical displacement values with μm accuracy. The solid line in Figure 15. is not able to approximate any kind of definite regression functions with required precision. The solution was the following: let calculate the logarithm (base: 10) of both parameters, i.e. vertical displacement and α_{srh}. Figure 16. shows an example for that related to the whole $100\ldots10^6$ kNm/rad interval. After trying the application of this kind of regression function it had to be stated that the deviation is too high, and the min. 10^{-2} mm accuracy can't be guaranteed (μm precision was neglected because it is unreal requirement for this wide interval). The final solution was that only the $100\ldots30000$ kNm/rad range was considered and the polynomial regression functions (with maximum 5th power) then calculated for all the cases (see Figure 17.).

It should be mentioned that in all published regression function the 'x' is the independent factor and 'y' is the independent.
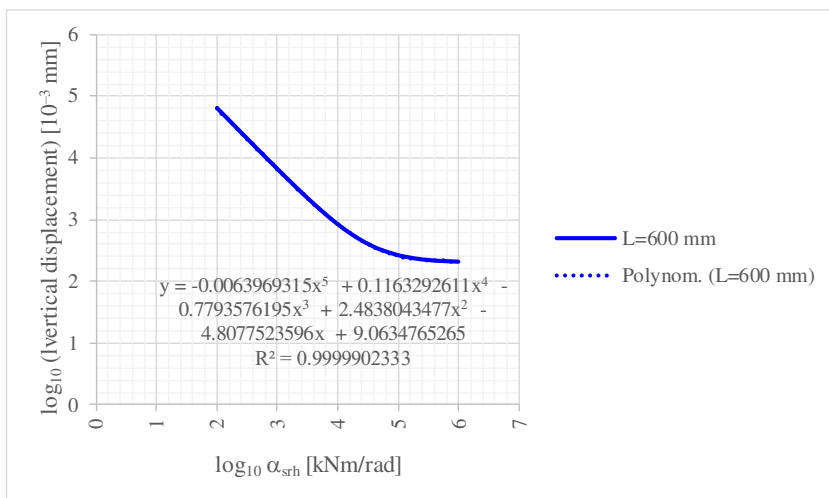
Figure 16.   Logarithm (base: 10) of vertical displacement as a function of logarithm (base: 10) α_{srh} in case of fishplated rail joint with 60E1 rail profile and L=600 mm bay length related to $\alpha_{srh}=100\ldots10^6$ kNm/rad
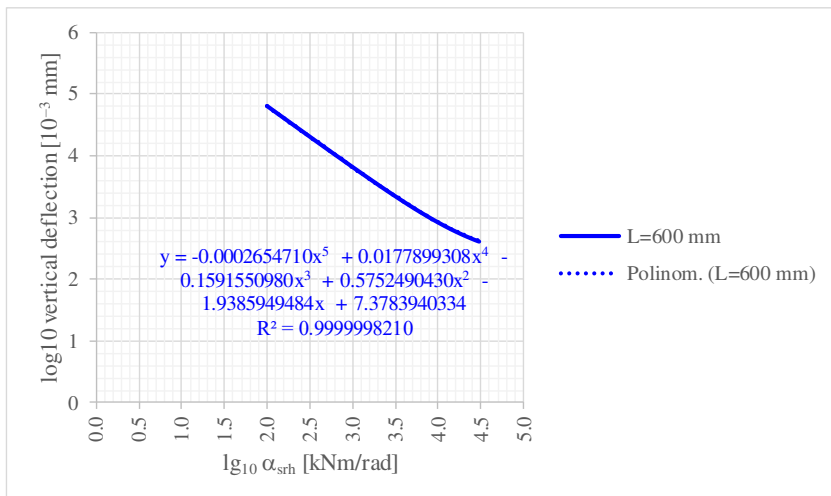
Figure 17. *Logarithm (base: 10) of vertical displacement as a function of logarithm (base: 10) α_{srh} in case of fishplated rail joint with 60E1 rail profile and L=600 mm bay length related to α_{srh}=100…30000 kNm/rad*

In Tables 9-23. the authors give all the applicable regression functions with the determination of average deviation from the accurate value for the range α_{srh}=100…30000 kNm/rad. The unit of vertical displacement is 10^{-3} mm in the equations.

Table 9. Calculated regression functions related to fishplated rail joints with 60E1 rail profile – Results I.

	independent factor: $log_{10}\alpha_{srh}$, dependent factor: log_{10}(vertical displacement)			independent factor: log_{10}(vertical displacement), dependent factor: $log_{10}\alpha_{srh}$		
	regression function	*R^2*	*average of deviation*	*regression function*	*R^2*	*average of deviation*
L=600 mm	$y = -0.0002654710x^5 + 0.0177899308x^4 - 0.1591550980x^3 + 0.5752490430x^2 - 1.9385949484x + 7.3783940334$	$R^2 = 0.9999998210$	0.0000221236%	$y = -0.0561899853x^5 + 1.1032436012x^4 - 8.6385175383x^3 + 33.7592428687x^2 - 66.9611874383x + 58.4830806693$	$R^2 = 0.9999957935$	0.0005154704%

Table 10. *Calculated regression functions related to fishplated rail joints with 60E1 rail profile – Results II.*

			L=850 mm	L=800 mm	L=750 mm	L=700 mm	L=650 mm
independent factor: $\log_{10}\alpha_{th}$, *dependent factor:* $\log_{10}($*vertical displacement*$)$	*regression function*		y = −0.0033210359x^5 + 0.0661958110x^4 − 0.4528912154x^3 + 1.4428644548x^2 − 3.1925229984x + 8.2408506561	y = −0.0028220518x^5 + 0.0584314969x^4 − 0.4067582290x^3 + 1.3095351558x^2 − 3.0039610732x + 8.1097985517	y = −0.0021432178x^5 + 0.0478409864x^4 − 0.3432131942x^3 + 1.1235846853x^2 − 2.7373624996x + 7.9316165996	y = −0.0013927717x^5 + 0.0357334421x^4 − 0.2680392521x^3 + 0.8960634459x^2 − 2.4004218821x + 7.7060296338	y = −0.0008675869x^5 + 0.0274169554x^4 − 0.2179124883x^3 + 0.7494551986x^2 − 2.1909850801x + 7.5565332083
	R^2		$R^2 = 0.9999997432$	$R^2 = 0.9999997523$	$R^2 = 0.9999997691$	$R^2 = 0.9999998301$	$R^2 = 0.9999998201$
	average of deviation		0.0000146938%	0.0000289608%	0.0000278861%	0.0000171485%	0.0000238425%
independent factor: $\log_{10}($*vertical displacement*$)$, *dependent factor:* $\log_{10}\alpha_{th}$	*regression function*		y = −0.1012860202x^5 + 2.0716604518x^4 − 16.8938387765x^3 + 68.7142814229x^2 − 140.5706088567x + 120.4079627696	y = −0.0907265018x^5 + 1.8429006315x^4 − 14.9255519735x^3 + 60.2995245135x^2 − 122.6773526942x + 105.2303094370	y = −0.0820717992x^5 + 1.6540633765x^4 − 13.2914009039x^3 + 53.2806372990x^2 − 107.6948172465x + 92.456046536	y = −0.0725327943x^5 + 1.4499957163x^4 − 11.5583749154x^3 + 45.9706429550x^2 − 92.3619217437x + 79.611783186	y = −0.0640422302x^5 + 1.2692465779x^4 − 10.0311434430x^3 + 39.5613555266x^2 − 78.9843113711x + 68.459335125
	R^2		$R^2 = 0.9999895033$	$R^2 = 0.9999911790$	$R^2 = 0.9999925232$	$R^2 = 0.9999934870$	$R^2 = 0.9999949108$
	average of deviation		0.0012791697%	0.0010810201%	0.0009099702%	0.0007953655%	0.0006262364%

Table 11. Calculated regression functions related to fishplated rail joints with 60E1 rail profile – Results III.

			L=1050 mm	L=1000 mm	L=950 mm	L=900 mm
independent factor: $\log_{10}\alpha_{rh}$, dependent factor: $\log_{10}$(vertical displacement)	regression function		y = −0.0056866782x^5 + 0.1026925116x^4 − 0.6695917095x^3 + 2.0711949825x^2 − 4.0861892133x + 8.8324734791	y = −0.0053150810x^5 + 0.0971002356x^4 − 0.6375935145x^3 + 1.9821967514x^2 − 3.9650156584x + 8.7464165945	y = −0.0046061362x^5 + 0.0861421522x^4 − 0.5721531139x^3 + 1.7911127715x^2 − 3.6912232257x + 8.5698764230	y = −0.0040329075x^5 + 0.0773380185x^4 − 0.5201728782x^3 + 1.6413265320x^2 − 3.4795516660x + 8.4287791081
		R^2	$R^2 = 0.9999996743$	$R^2 = 0.9999996713$	$R^2 = 0.9999996928$	$R^2 = 0.9999997130$
		average of deviation	0.0000164671%	0.0000229532%	0.0000270493%	0.0000133017%
independent factor: $\log_{10}$(vertical displacement), dependent factor: $\log_{10}\alpha_{rh}$	regression function		y = −0.1454994555x^5 + 3.0519049696x^4 − 25.5218121825x^3 + 106.4321590274x^2 − 222.5440456531x + 191.4416157790	y = −0.1326680665x^5 + 2.7673588452x^4 − 23.0147266832x^3 + 95.4542635987x^2 − 198.6354482460x + 170.6798940424	y = −0.1219586286x^5 + 2.5280618612x^4 − 20.8929220814x^3 + 86.1138235732x^2 − 178.2009767155x + 152.8615621321	y = −0.1114528745x^5 + 2.2954577137x^4 − 18.8488088772x^3 + 77.1934338616x^2 − 158.8499783286x + 136.1227490645
		R^2	$R^2 = 0.9999818273$	$R^2 = 0.9999845914$	$R^2 = 0.9999861540$	$R^2 = 0.9999879868$
		average of deviation	0.0022247493%	0.0018896224%	0.0016955949%	0.0014735703%

L=1250 mm	L=1200 mm	L=1150 mm	L=1100 mm
$y = -0.0078476353x^5 + 0.1354758318x^4 - 0.8613427044x^3 + 2.6199056929x^2 - 4.8576459021x + 9.3353738748$	$y = -0.0071632130x^5 + 0.1250176055x^4 - 0.7993670023x^3 + 2.4398173790x^2 - 4.6003185666x + 9.1728313689$	$y = -0.0066581481x^5 + 0.1173905492x^4 - 0.7550208157x^3 + 2.3137212004x^2 - 4.4241748344x + 9.0574324083$	$y = -0.0062391696x^5 + 0.1111953507x^4 - 0.7200503120x^3 + 2.2177097626x^2 - 4.2951932263x + 8.9700551252$
$R^2 = 0.9999996221$	$R^2 = 0.9999996596$	$R^2 = 0.9999996765$	$R^2 = 0.9999996450$
0.0000288602%	0.0000307143%	0.0000350885%	0.0000363338%
$y = -0.1971880330x^5 + 4.2232804742x^4 - 36.0633859512x^3 + 153.5557937789x^2 - 327.2683984822x + 284.1692006955$	$y = -0.1846161577x^5 + 3.9340319900x^4 - 33.4226763958x^3 + 141.5881363130x^2 - 300.3210904444x + 260.0095253571$	$y = -0.1710676902x^5 + 3.6269146123x^4 - 30.6576269091x^3 + 129.2206381315x^2 - 272.8185085350x + 235.6421280429$	$y = -0.1583223973x^5 + 3.3391009431x^4 - 28.0765704616x^3 + 117.7225441042x^2 - 247.3529795149x + 213.1680563088$
$R^2 = 0.9999725112$	$R^2 = 0.9999741824$	$R^2 = 0.9999768156$	$R^2 = 0.9999795691$
0.0033553501%	0.0031528096%	0.0028324250%	0.0024941816%

Table 12. Calculated regression functions related to fishplated rail joints with 60E1 rail profile – Results IV.

	independent factor: $\log_{10}\alpha_{th}$, dependent factor: $\log_{10}$(vertical displacement)			independent factor: $\log_{10}$(vertical displacement), dependent factor: $\log_{10}\alpha_{th}$		
	regression function	R²	average of deviation	regression function	R²	average of deviation
L=1300 mm	y = –0.0082576624x^5 + 0.1415842390x^4 – 0.8962501747x^3 + 2.7173674164x^2 – 4.9913025011x + 9.4246203085	R² = 0.9999996302	0.0000342679%	y = –0.2122735276x^5 + 4.5673264466x^4 – 39.1811129147x^3 + 167.5962033750x^2 – 358.7118267247x + 312.2236849620	R² = 0.9999691675	0.0037744853%
L=1350 mm	y = –0.0086414902x^5 + 0.1472166789x^4 – 0.9278953607x^3 + 2.8041375371x^2 – 5.1080813253x + 9.5029174845	R² = 0.9999996340	0.0000213951%	y = –0.2273828567x^5 + 4.9141999545x^4 – 42.3449253947x^3 + 181.9354675484x^2 – 391.0272836760x + 341.2340542740	R² = 0.9999659443	0.0041564983%
L=1400 mm	y = –0.0090165159x^5 + 0.1526885200x^4 – 0.9584609427x^3 + 2.8874814768x^2 – 5.2196620702x + 9.5775891304	R² = 0.9999996239	0.0000152342%	y = –0.2428640641x^5 + 5.2714413529x^4 – 45.6200177431x^3 + 196.8548606502x^2 – 424.8205280148x + 371.7215253419	R² = 0.9999626904	0.0045635781%

Table 13.   *Calculated regression functions related to fishplated rail joints with 60E1 rail profile – Results V.*

	independent factor: $\log_{10}\alpha_{srh}$, dependent factor: $\log_{10}$(vertical displacement)			independent factor: $\log_{10}$(vertical displacement), dependent factor: $\log_{10}\alpha_{srh}$		
	regression function	R^2	*average of deviation*	*regression function*	R^2	*average of deviation*
L=1450 mm	y = −0.0093630010x^5 + 0.1577577333x^4 − 0.9868358788x^3 + 2.9650745426x^2 − 5.3237741431x + 9.6479177960	$R^2 = 0.9999996269$	0.0000132456%	y = −0.2598413088x^5 + 5.6630712851x^4 − 49.2106101098x^3 + 213.2178702378x^2 − 461.9072287493x + 405.2049754741	$R^2 = 0.9999587516$	0.0050353778%
L=1490 mm	y = −0.0098311942x^5 + 0.1647822548x^4 − 1.0277118568x^3 + 3.0817926441x^2 − 5.4879693614x + 9.7507898574	$R^2 = 0.9999996313$	0.0000301588%	y = −0.2714433404x^5 + 5.9360274175x^4 − 51.7591717106x^3 + 225.0312032245x^2 − 489.1128875121x + 430.1410210140	$R^2 = 0.9999571607$	0.0052305715%

Table 14.   *Calculated regression functions related to fishplated rail joints with 54E1 rail profile – Results I.*

	independent factor: $\log_{10}\alpha_{xh}$, *dependent factor:* $\log_{10}$(*vertical displacement*)			*independent factor:* $\log_{10}$(*vertical displacement*), *dependent factor:* $\log_{10}\alpha_{xh}$		
	regression function	R^2	*average of deviation*	*regression function*	R^2	*average of deviation*
L=600 mm	y = −0.0023950942x^5 + 0.0517286448x^4 − 0.3661582143x^3 + 1.1894903556x^2 − 2.8300674899x + 7.8674378901	R² = 0.9999997140	0.0000143668%	y = −0.0861539520x^5 + 1.6870998286x^4 − 13.1695500618x^3 + 51.2760141306x^2 − 100.7274110563x + 84.4646453939	R² = 0.9999919243	0.0009846443%
L=650 mm	y = −0.0031363651x^5 + 0.0632291803x^4 − 0.4345140009x^3 + 1.3873063173x^2 − 3.1102823414x + 8.0580729475	R² = 0.9999997254	0.0000203742%	y = −0.0983669709x^5 + 1.9453085657x^4 − 15.3350142482x^3 + 60.2904780777x^2 − 119.3782314121x + 99.8680081882	R² = 0.9999897273	0.0012518941%
L=700 mm	y = −0.0041832537x^5 + 0.0796865374x^4 − 0.5345425339x^3 + 1.6844469858x^2 − 3.5430279180x + 8.3377769213	R² = 0.9999996662	0.0000201715%	y = −0.1111043963x^5 + 2.2179077826x^4 − 17.6485721672x^3 + 70.0339079914x^2 − 139.7650194615x + 116.8806261792	R² = 0.9999881388	0.0014497490%
L=750 mm	y = −0.0048361347x^5 + 0.0896370423x^4 − 0.5926091681x^3 + 1.8494869542x^2 − 3.7727837858x + 8.4934602363	R² = 0.9999997040	0.0000143839%	y = −0.1250508675x^5 + 2.5173609203x^4 − 20.2001709778x^3 + 80.8288349936x^2 − 162.4648252392x + 135.9174722841	R² = 0.9999854956	0.0017747124%

Table 15.   Calculated regression functions related to fishplated rail joints with 54E1 rail profile – Results II.

| | independent factor: $\log_{10}\alpha_{th}$, dependent factor: $\log_{10}($vertical displacement$)$ | | | independent factor: $\log_{10}($vertical displacement$)$, dependent factor: $\log_{10}\alpha_{th}$ | | |
	regression function	R²	average of deviation	regression function	R²	average of deviation
L=800 mm	y = −0.0054737103x^5 + 0.0993992174x^4 − 0.6499935139x^3 + 2.0142186664x^2 − 4.0049106689x + 8.6502436902	R² = 0.9999996557	0.0000212083%	y = −0.1403612071x^5 + 2.8476041778x^4 − 23.0279502680x^3 + 92.8536858921x^2 − 187.8839158021x + 157.3409428353	R² = 0.9999826167	0.0021262458%
L=850 mm	y = −0.0061280490x^5 + 0.1093521455x^4 − 0.7081660603x^3 + 2.1802514819x^2 − 4.2374631701x + 8.8047788808	R² = 0.9999996785	0.0000209281%	y = −0.1564027874x^5 + 3.1965383251x^4 − 26.0409880597x^3 + 105.7740669105x^2 − 215.4233058702x + 180.7361809750	R² = 0.9999795365	0.0025008189%
L=900 mm	y = −0.0066711128x^5 + 0.1174908352x^4 − 0.7548613789x^3 + 2.3109446742x^2 − 4.4169221231x + 8.9266108706	R² = 0.9999996846	0.0000211430%	y = −0.1735010395x^5 + 3.5704974174x^4 − 29.2884981967x^3 + 119.7812570017x^2 − 245.4560746816x + 206.3966225772	R² = 0.9999758698	0.0029520647%
L=950 mm	y = −0.0074204477x^5 + 0.1289111816x^4 − 0.8220961146x^3 + 2.5047122118x^2 − 4.6913067761x + 9.1030661431	R² = 0.9999996569	0.0000201606%	y = −0.1909290496x^5 + 3.9556426373x^4 − 32.6671256126x^3 + 134.4982800941x^2 − 277.3146762908x + 233.8674558251	R² = 0.9999726882	0.0033425266%

Table 16. Calculated regression functions related to fishplated rail joints with 54E1 rail profile – Results III.

	L=1000 mm	L=1050 mm	L=1100 mm	L=1150 mm
regression function (independent factor: $\log_{10}\alpha_{rh}$, dependent factor: $\log_{10}$(vertical displacement))	y = −0.0082757423x^5 + 0.1420087585x^4 − 0.8999040420x^3 + 2.7314808277x^2 − 5.0164291564x + 9.3089490289	y = −0.0086827679x^5 + 0.1478508963x^4 − 0.9316813315x^3 + 2.8152164580x^2 − 5.1240009332x + 9.3842463176	y = −0.0091911735x^5 + 0.1552909560x^4 − 0.9734311260x^3 + 2.9296345647x^2 − 5.2779841688x + 9.4861232228	y = −0.0097281332x^5 + 0.1631810090x^4 − 1.0180218542x^3 + 3.0529191399x^2 − 5.4455499391x + 9.5952295343
R^2	R² = 0.9999995798	R² = 0.9999996160	R² = 0.9999996358	R² = 0.9999996194
average of deviation	0.0000223430%	0.0000305542%	0.0000357739%	0.0000384051%
regression function (independent factor: $\log_{10}$(vertical displacement), dependent factor: $\log_{10}\alpha_{rh}$)	y = −0.2084629156x^5 + 4.3468634050x^4 − 36.1313212843x^3 + 149.7267789861x^2 − 310.5770683909x + 262.7982781940	y = −0.2280493770x^5 + 4.7833856373x^4 − 39.9952826607x^3 + 166.7175894291x^2 − 347.7189261798x + 295.1387452784	y = −0.2479546435x^5 + 5.2305830618x^4 − 43.9850574642x^3 + 184.3982638655x^2 − 386.6648272966x + 329.3023713399	y = −0.2684199311x^5 + 5.6934063934x^4 − 48.1414089346x^3 + 202.9374106941x^2 − 427.7656895694x + 365.5836120802
R^2	R² = 0.9999704686	R² = 0.9999656654	R² = 0.9999616774	R² = 0.9999576246
average of deviation	0.0036060012%	0.0041904290%	0.0046871027%	0.0051768130%

Table 17.   Calculated regression functions related to fishplated rail joints with 54E1 rail profile – Results IV.

	independent factor: $\log_{10}\alpha_{cth}$, dependent factor: $\log_{10}(vertical\ displacement)$			independent factor: $\log_{10}(vertical\ displacement)$, dependent factor: $\log_{10}\alpha_{cth}$		
	regression function	R²	average of deviation	regression function	R²	average of deviation
L=1200 mm	y = −0.0103177967x^5 + 0.1719785129x^4 − 1.0687746471x^3 + 3.1966782997x^2 − 5.6462461298x + 9.7243568183	R² = 0.9999995896	0.0000371832%	y = −0.2902143466x^5 + 6.1881351269x^4 − 52.6017564564x^3 + 222.9135219596x^2 − 472.2366007985x + 405.0019462667	R² = 0.9999536694	0.0056638874%
L=1250 mm	y = −0.0106695760x^5 + 0.1769233708x^4 − 1.0951057087x^3 + 3.2646700975x^2 − 5.7319120916x + 9.7843636293	R² = 0.9999996104	0.0000272666%	y = −0.3133936708x^5 + 6.7153786504x^4 − 57.3666411479x^3 + 244.3109297159x^2 − 520.0110812186x + 447.4778748520	R² = 0.9999483973	0.0063012506%
L=1300 mm	y = −0.0109614626x^5 + 0.1808664192x^4 − 1.1149330206x^3 + 3.3121177763x^2 − 5.7859643811x + 9.8247073820	R² = 0.9999996384	0.0000336852%	y = −0.3371669283x^5 + 7.2592153862x^4 − 62.3094592053x^3 + 266.6334432367x^2 − 570.1330149101x + 492.2893470980	R² = 0.9999425599	0.0070189160%
L=1350 mm	y = −0.0113193429x^5 + 0.1858899807x^4 − 1.1417561401x^3 + 3.3818193287x^2 − 5.8746656760x + 9.8855127794	R² = 0.9999996616	0.0000187861%	y = −0.3615386726x^5 + 7.8199321228x^4 − 67.4345712312x^3 + 289.9091322752x^2 − 622.6852863336x + 539.5291834828	R² = 0.9999372772	0.0076584546%

Table 18. Calculated regression functions related to fishplated rail joints with 54E1 rail profile – Results V.

	independent factor: $\log_{10}\alpha_{th}$, dependent factor: $\log_{10}$(vertical displacement)) — regression function	R^2	average of deviation	independent factor: $\log_{10}$(vertical displacement), dependent factor: $\log_{10}\alpha_{th}$ — regression function	R^2	average of deviation
L=1400 mm	$y = -0.0116752077x^5 + 0.1908810210x^4 - 1.1683671006x^3 + 3.4507763688x^2 - 5.9619998838x + 9.9446782348$	$R^2 = 0.9999996664$	0.0000175928%	$y = -0.3873424040x^5 + 8.4154163492x^4 - 72.8952060741x^3 + 314.7931315310x^2 - 679.0663641808x + 590.3900130294$	$R^2 = 0.9999311269$	0.0084264457%
L=1450 mm	$y = -0.0118300935x^5 + 0.1926352784x^4 - 1.1746195692x^3 + 3.4571903883x^2 - 5.9554490824x + 9.9482155621$	$R^2 = 0.9999997167$	0.0000297278%	$y = -0.4140292777x^5 + 9.0333937851x^4 - 78.5823039135x^3 + 340.8045857499x^2 - 738.2251372030x + 643.9616332720$	$R^2 = 0.9999239653$	0.0092839177%
L=1490 mm	$y = -0.0122201483x^5 + 0.1982840048x^4 - 1.2062237366x^3 + 3.5440513997x^2 - 6.0731969245x + 10.0231168651$	$R^2 = 0.9999997033$	0.0000122504%	$y = -0.4340632780x^5 + 9.5029318517x^4 - 82.9524577908x^3 + 361.0071339340x^2 - 784.6402905282x + 686.4002091336$	$R^2 = 0.9999208276$	0.0096796514%

Table 19.   *Calculated regression functions related to fishplated rail joints with MÁV 48.5 rail profile – Results I.*

	independent factor: $\log_{10}\alpha_{th}$, dependent factor: $\log_{10}$(vertical displacement)			independent factor: $\log_{10}$(vertical displacement), dependent factor: $\log_{10}\alpha_{th}$		
	regression function	R^2	average of deviation	regression function	R^2	average of deviation
L=600 mm	$y = -0.0057814279x^5 + 0.1042846122x^4 - 0.6801995279x^3 + 2.1056504833x^2 - 4.1405616481x + 8.5335059579$	$R^2 = 0.9999995915$	0.0000209688%	$y = -0.1428358092x^5 + 2.7589781137x^4 - 21.2345567809x^3 + 81.4690008045x^2 - 157.0029384151x + 126.2102719554$	$R^2 = 0.9999824582$	0.0021465455%
L=650 mm	$y = -0.0066426031x^5 + 0.1173308335x^4 - 0.7561163405x^3 + 2.3213242044x^2 - 4.4411676436x + 8.7331371228$	$R^2 = 0.9999995805$	0.0000346717%	$y = -0.1645552317x^5 + 3.2113295290x^4 - 24.9715457912x^3 + 96.7896713559x^2 - 188.2062315091x + 151.5360778317$	$R^2 = 0.9999779670$	0.0026926435%
L=700 mm	$y = -0.0074295557x^5 + 0.1292130956x^4 - 0.8250834934x^3 + 2.5171315494x^2 - 4.7144717872x + 8.9156990314$	$R^2 = 0.9999995717$	0.0000215097%	$y = -0.1889770818x^5 + 3.7224289841x^4 - 29.2166340917x^3 + 114.2945338847x^2 - 224.0751786054x + 180.8214394738$	$R^2 = 0.9999736089$	0.0032303653%
L=750 mm	$y = -0.0081845015x^5 + 0.1404361222x^4 - 0.8891233641x^3 + 2.6955919415x^2 - 4.9586121756x + 9.0772129764$	$R^2 = 0.9999996083$	0.0000213983%	$y = -0.2137360964x^5 + 4.2477709302x^4 - 33.6390483282x^3 + 132.7715751245x^2 - 262.4241496730x + 212.5183902188$	$R^2 = 0.9999681082$	0.0038931699%

Table 20. *Calculated regression functions related to fishplated rail joints with MÁV 48.5 rail profile – Results II.*

independent factor: $\log_{10}\alpha_{eh}$, dependent factor: $\log_{10}$(vertical displacement)

	L=800 mm	L=850 mm	L=900 mm	L=950 mm
regression function	y = −0.0088384119x^5 + 0.1499403932x^4 − 0.9419171100x^3 + 2.8384704707x^2 − 5.1481323929x + 9.2041632551	y = −0.0096809028x^5 + 0.1625812006x^4 − 1.0152733697x^3 + 3.0473979868x^2 − 5.4412278568x + 9.3927314723	y = −0.0101146611x^5 + 0.1685782631x^4 − 1.0463432705x^3 + 3.1246015071x^2 − 5.5336100766x + 9.4601861979	y = −0.0106906622x^5 + 0.1768005025x^4 − 1.0912344537x^3 + 3.2442409853x^2 − 5.6901850552x + 9.5644522994
R^2	R² = 0.9999996130	R² = 0.9999995705	R² = 0.9999996405	R² = 0.9999996449
average of deviation	0.0000433849%	0.0000220629%	0.0000152518%	0.0000313510%

independent factor: $\log_{10}$(vertical displacement), dependent factor: $\log_{10}\alpha_{eh}$

	L=800 mm	L=850 mm	L=900 mm	L=950 mm
regression function	y = −0.2397670668x^5 + 4.8047659307x^4 − 38.3682288473x^3 + 152.7024680575x^2 − 304.1538305301x + 247.3073666691	y = −0.2675203988x^5 + 5.4031378463x^4 − 43.4878649139x^3 + 174.4460638485x^2 − 350.0306697924x + 285.8408684041	y = −0.2977939485x^5 + 6.0584605864x^4 − 49.1197307436x^3 + 198.4803628324x^2 − 400.9990779617x + 328.8722307656	y = −0.3281155159x^5 + 6.7220861170x^4 − 54.8845269282x^3 + 223.3419611326x^2 − 454.2681040467x + 374.2994152220
R^2	R² = 0.9999626241	R² = 0.9999578425	R² = 0.9999499385	R² = 0.9999437975
average of deviation	0.0045700822%	0.0051495222%	0.0061214414%	0.0068710977%

Table 21.   Calculated regression functions related to fishplated rail joints with MÁV 48.5 rail profile – Results III.

	independent factor: $\log_{10}\alpha_{th}$, dependent factor: $\log_{10}$(vertical displacement)			independent factor: $\log_{10}$(vertical displacement), dependent factor: $\log_{10}\alpha_{th}$		
	regression function	R^2	average of deviation	regression function	R^2	average of deviation
L=1000 mm	$y = -0.0112954756x^5 + 0.1855398384x^4 - 1.1397731430x^3 + 3.3762994708x^2 - 5.8670832851x + 9.6803138335$	$R^2 = 0.9999996629$	0.0000299307%	$y = -0.3601000160x^5 + 7.4265510861x^4 - 61.0435791343x^3 + 250.0771286454x^2 - 511.9266877604x + 423.7871367899$	$R^2 = 0.9999373223$	0.0076617258%
L=1050 mm	$y = -0.0117380912x^5 + 0.1916586514x^4 - 1.1717861820x^3 + 3.4574428702x^2 - 5.9672887901x + 9.7498965394$	$R^2 = 0.9999996733$	0.0000270966%	$y = -0.3944556535x^5 + 8.1860616618x^4 - 67.7110319210x^3 + 279.1461331718x^2 - 574.9085597462x + 478.0997795910$	$R^2 = 0.9999297517$	0.0076617258%
L=1100 mm	$y = -0.0121514024x^5 + 0.1972532179x^4 - 1.2002408684x^3 + 3.5269575234x^2 - 6.0490987512x + 9.8071970165$	$R^2 = 0.9999996937$	0.0000177270%	$y = -0.4293009544x^5 + 8.9628422529x^4 - 74.5862718536x^3 + 309.3647641823x^2 - 640.9067588044x + 535.4615174595$	$R^2 = 0.9999221558$	0.0095171965%
L=1150 mm	$y = -0.0125237394x^5 + 0.2023349235x^4 - 1.2264118002x^3 + 3.5922755185x^2 - 6.1286007862x + 9.8643920318$	$R^2 = 0.9999996992$	0.0000218575%	$y = -0.4683178528x^5 + 9.8326144100x^4 - 82.2890819118x^3 + 343.2570114440x^2 - 715.0361119465x + 599.9997095024$	$R^2 = 0.9999132806$	0.0106053111%

A. Németh et al. – Acta Technica Jaurinensis, Vol. 13, No. 1, pp. 42-84, 2020

Table 22.   *Calculated regression functions related to fishplated rail joints with MÁV 48.5 rail profile – Results IV.*

	L=1200 mm	L=1250 mm	L=1300 mm	L=1350 mm
independent factor: $\log_{10}\alpha_{th}$, dependent factor: $\log_{10}$(vertical displacement)				
regression function	$y = -0.0129051950x^5 + 0.2074734921x^4 - 1.2524710542x^3 + 3.6560010408x^2 - 6.2040414473x + 9.9175028562$	$y = -0.0136918364x^5 + 0.2199597155x^4 - 1.3308257421x^3 + 3.9016880433x^2 - 6.5879093045x + 10.1726997485$	$y = -0.0133216277x^5 + 0.2122579884x^4 - 1.2705729106x^3 + 3.6803621642x^2 - 6.2019172573x + 9.9325180113$	$y = -0.0135832661x^5 + 0.2155848665x^4 - 1.2860675243x^3 + 3.7141815411x^2 - 6.2360879521x + 9.9612416000$
R^2	$R^2 = 0.9999997416$	$R^2 = 0.9999993560$	$R^2 = 0.9999997918$	$R^2 = 0.9999997849$
average of deviation	0.0000037833%	0.0000473591%	0.0000234743%	0.0000006003%
independent factor: $\log_{10}$(vertical displacement), dependent factor: $\log_{10}\alpha_{th}$				
regression function	$y = -0.5066505843x^5 + 10.6960124471x^4 - 90.0121127966x^3 + 377.5686812397x^2 - 790.7928995171x + 666.5614190845$	$y = -0.5474912254x^5 + 11.6205418503x^4 - 98.3219347941x^3 + 414.6588017709x^2 - 873.0507778459x + 739.1447603909$	$y = -0.5902008603x^5 + 12.5876363697x^4 - 107.0265467178x^3 + 453.6035302115x^2 - 959.6980573317x + 815.8949805144$	$y = -0.6350512881x^5 + 13.6092228569x^4 - 116.2728291680x^3 + 495.1892230924x^2 - 1,052.6826466440x + 898.6475726086$
R^2	$R^2 = 0.9999051853$	$R^2 = 0.9998954373$	$R^2 = 0.9998850622$	$R^2 = 0.9998754005$
average of deviation	0.0115931097%	0.0127785372%	0.0127785372%	0.0152278570%

Table 23.   *Calculated regression functions related to fishplated rail joints with MÁV 48.5 rail profile – Results V.*

	independent factor: $\log_{10}\alpha_{srh}$, dependent factor: $\log_{10}$(vertical displacement)			independent factor: $\log_{10}$(vertical displacement), dependent factor: $\log_{10}\alpha_{srh}$		
	regression function	R^2	average of deviation	regression function	R^2	average of deviation
L=1400 mm	$y = -0.0137478114x^5 + 0.2172123771x^4 - 1.2900436827x^3 + 3.7101257329x^2 - 6.2098060550x + 9.519169125$	$R^2 = 0.9999998146$	0.0000000795%	$y = -0.6779067673x^5 + 14.5961821106x^4 - 125.2994345539x^3 + 536.1998393772x^2 - 1,145.2752803575x + 981.8278260078$	$R^2 = 0.9998662167$	0.0163527686%
L=1450 mm	$y = -0.0138543464x^5 + 0.2180991237x^4 - 1.2905542882x^3 + 3.6989300886x^2 - 6.1777298683x + 9.9412739728$	$R^2 = 0.9999998343$	0.0000013880%	$y = -0.7275428193x^5 + 15.7340264150x^4 - 135.6684742503x^3 + 583.1652358119x^2 - 1,251.0656837793x + 1,076.6897021461$	$R^2 = 0.9998541343$	0.0178360257%
L=1490 mm	$y = -0.0138689191x^5 + 0.2176407902x^4 - 1.2834172636x^3 + 3.6661259816x^2 - 6.1152272934x + 9.9101504118$	$R^2 = 0.9999998673$	0.0000164799%	$y = -0.7678739279x^5 + 16.6633018955x^4 - 144.1793936536x^3 + 621.9104066674x^2 - 1,338.7758603483x + 1,155.7277883590$	$R^2 = 0.9998435939$	0.0191063579%

6. Conclusions

The authors introduced and detailed a possibility to be able to model glued insulated rail joints in FEM software. A simple 2-D FEM model was applied for all the cases that has only one factor to be set. This factor is the α_{srh} rigidity of the semi-rigid hinge that simulates the rotation (bending) behaviour of the fishplated rail joints in the middle zone. Only the investigated glued insulated rail joints with glass-fibre reinforced fishplates were considered in this article.

A lot of running and a very long, time consuming calibration process had to be executed.

After calibration the models should be validated. The authors use two different validation methods (cases). The built and calibrated FEM models were able to be validated.

The authors determined and published special regression functions:

- vertical displacement vs. bay lengths for different α_{srh} values,
- vertical displacement vs. α_{srh} values for different bay lengths,
- α_{srh} values vs. vertical displacement for different bay lengths.

These can be used for quick calculation without FEM simulations.

In the future the authors would like to expand this method for model not only polymer-composite fishplated glued insulated rail joints but with steel fishplates, as well as insulated rail joints (i.e. without glue), etc. The results can be compared on wider range than from the laboratory tests. There is other plan to compose FEM models to be able to simulate longer railway track sections with different support characteristics. The results from the longer railway tracks' FEM model are able to be set against the field tests [39] [40] [41] [44].

Acknowledgements

References

[1]   M. Gallou, B. Temple et al., Potential for external reinforcement of insulated rail joints, Proceedings of the Institution of Mechanical Engineers, Part F: Journal of Rail and Rapid Transit 232 (3) (2018) pp. 697–708.
doi: *https://doi.org/10.1177/0954409716684278*

[2]   P. Boyd, N. Mandal et al., Experimental Investigation into The Failure Behaviour Of Insulated Rail Joints. Conference On Railway Engineering (CORE), Brisbane, 2012. 8 p.
URL
https://www.researchgate.net/publication/259240841_Experimental_investigation_into_the_failure_behaviour_of_insulated_rail_joints

[3]   E. Soylemez, K. Ciloglu, Influence of Track Variables and Product Design on Insulated Rail Joints. Transportation Research Record: Journal of the

Transportation Research Board, No. 2545 (1) (2016) pp. 1–10.
doi: *https://doi.org/10.3141/2545-01*

[4] Y. C. Chen, J. H. Kuang, Contact stress variations near the insulated rail joints. Institution of Mechanical Engineers, Part F: Journal of Rail and Rapid Transit 216 (4) (2002) pp. 265–273.
doi: *https://doi.org/10.1243/095440902321029217*

[5] P. Beaty, B. Temple et al., Experimental modelling of lipping in insulated rail joints and investigation of rail head material improvements. Proc IMechE Part F: Journal of Rail and Rapid Transit 230 (4) (2016) pp. 1375–1387.
doi: *https://doi.org/10.1177/0954409715600740*

[6] F. A. Elshukri, An Experimental Investigation and Improvement of Insulated Rail Joints (IRJs) End Post Performance. Ph.D. thesis, Faculty of Engineering of the University of Sheffield. Department of Mechanical Engineering. The University of Sheffield (2016).
URL *http://etheses.whiterose.ac.uk/id/eprint/12066*

[7] F. A. Elshukri, R. Lewis (2016): An Experimental Investigation and Improvement of Insulated Rail Joints. Tribology in Industry 38 (1) (2016) pp. 121–126.

[8] M. Dhanasekar, Research Outcomes for Improved Management of Insulated Rail Joints. Research outcomes for improved management of insulated rail joints. In Forde, M C (Ed.) Proceedings of the 13th Railway Engineering International Conference and Exhibition:. ECS Publications, Edinburgh, United Kingdom, 2015, pp. 1–14.
URL *https://eprints.qut.edu.au/85443/*

[9] F. A. Elshukri, R. Lewis, An Experimental Investigation And Improvement Of Insulated Rail Joints. Conference paper: 14th International Serbian Conference on Tribology Serbiatrib'15, at Serbia. University of Belgrade, Faculty of Mechanical Engineering, Belgrade, 2015, 8 p.
URL
https://www.researchgate.net/publication/280445054_An_Exp erimental_Investigation_and_Improvement_of_Insulated_Rail _Joints_IRJs

[10] J. Sandström, A. Ekberg, Numerical study of the mechanical deterioration of insulated rail joints. JRRT243. Proc. IMechE Vol. 223 Part F: Journal of Rail

and Rapid Transit. IMechE 2009. pp. 265–273.
doi: *https://doi.org/10.1243/09544097JRRT243*

[11] N. Zong, H. Askarinejad et al. (2013): Service Condition of Railroad Corridors around the Insulated Rail Joints. 2013 American Society of Civil Engineers. Journal Of Transportation Engineering (Asce) 139 (6) (2013) pp. 643–650.
doi: *https://doi.org/10.1061/(ASCE)TE.1943-5436.0000541*

[12] H. M. El-sayed, M. Lotfy et al. (2018): A three dimensional finite element analysis of insulated rail joints deterioration, Engineering Failure Analysis 91 (2018) pp. 201–215.
doi: *https://doi.org/10.1016/j.engfailanal.2018.04.042*

[13] S. R. Lewis, L. Lewis et al. (2017): Full-scale testing of laser clad railway track; Case study – Testing for wear, bend fatigue and insulated block joint lipping integrity, Wear 376–377, Part B (2017) pp. 1930–1937.
doi: *https://doi.org/10.1016/j.wear.2017.02.023*

[14] C. Rathod et al., Microstructural characterisation of railhead damage in insulated rail joints. Materials Science Forum 706-709 (2012) Trans Tech Publications, Switzerland, pp. 2937–2942.
doi: *https://doi.org/10.4028/www.scientific.net/MSF.706-709.2937*

[15] A. Wöhnhart, Description of insulated rail joint at ÖBB Infrastruktur. Insulated rail joints assembled with high strength bolts, ÖBB Infrastruktur, Vienna, 2011. 88 p. in German (original translation to Hungarian)

[16] D. C. Peltier, C. P. L. Barkan, Modeling The Effects Of Epoxy Debonding On Bonded Insulated Rail Joints Subjected To Longitudinal Loads. In: Proceedings of the Transportation Research Board 87th Annual Meeting, Washington DC, 2008, 25 p.
URL
*https://pdfs.semanticscholar.org/7a29/9f4d3a38db225c2f34c
d70f88094f5077917.pdf*

[17] N. Zong, M. Dhanasekar, Sleeper embedded insulated rail joints for minimising the number of modes of failure, Engineering Failure Analysis 76 (2017) pp 27–43.
doi: *https://doi.org/10.1016/j.engfailanal.2017.02.001*

[18] N. K. Mandal, B. Peach, An Engineering Analysis of Insulated Rail Joints: A General Perspective. International Journal of Engineering Science and Technology 2 (8) (2010) pp. 3964–3988.

[19] A. K. Himebaugh, R. H. Plaut, D. A. Dillard , Finite element analysis of bonded insulated rail joints. International Journal of Adhesion & Adhesives 28 (3) (2008) pp 142–150.
doi: *https://doi.org/10.1016/j.ijadhadh.2007.09.003*

[20] N. K. Mandal, Stress Analysis Of Joint Bars Of Insulated Rail Joints Due To Wheel/Rail Contact Loadings. Conference paper: The 11th International Conference on Contact Mechanics and Wear of Rail/Wheel Systems (CM2018), Delft, 2018, pp. 675–680.

[21] M. Gallou, M. Frost et al. (2018): Assessing the deflection behaviour of mechanical and insulated rail joints through finite element analysis. Proceedings of the Institution of Mechanical Engineers, Part F: Journal of Rail and Rapid Transit, 232(9), pp. 2290-2308.
doi: *https://doi.org/10.1177/0954409718766925*

[22] T. M. Bandula-Heva, M. Dhanasekar, P. Boyd, Experimental Investigation of Wheel/Rail Rolling Contact at Railhead Edge. Experimental Mechanics 53 (2013) pp. 943–957.
doi: *https://doi.org/10.1007/s11340-012-9701-6*

[23] N. Zong, D. Wexler, M. Dhanasekar, Structural and Material Characterisation of Insulated Rail Joints, eJSE International. Special Issue: Electronic Journal of Structural Engineering 13 (1) (2013) pp. 75–87.

[24] Z. Yang, A. Boogaard et al., Numerical study of wheel-rail impact contact solutions at an insulated rail joint. International Journal of Mechanical Sciences 138-139 (2018) pp. 310–322.
doi: *https://doi.org/10.1016/j.ijmecsci.2018.02.025*

[25] H. Askarinejad, M. Dhanasekar (2015): Minimising The Failure Of Rail Joints Through Managing The Localised Condition Of Track. Railway Engineering 2015 Conference, Edinburgh, 2015, 9 p.
URL
https://www.researchgate.net/publication/280843973_MINIMI SING_THE_FAILURE_OF_RAIL_JOINTS_THROUGH_MANAGING_THE_LOCA LISED_CONDITION_OF_TRACK

[26] Z. Yang, X. Deng, Z. Li, Numerical modeling of dynamic frictional rolling contact with an explicit finite element method, Tribology International 129 (2018) pp. 214–231.
doi: *https://doi.org/10.1016/j.triboint.2018.08.028*

[27] V. Kovalchuk, M. Sysyn et al., Experimental investigation of the influence of train velocity and travel direction on the dynamic behavior of stiff common crossings, Facta Universitatis, Series: Mechanical Engineering 17 (3) (2019) pp. 345–356
doi: *https://doi.org/10.22190/FUME190514042K*

[28] M. Sysyn, F. Kluge et al. (2019) Experimental Analysis of Rail Contact Fatigue Damage on Frog Rail of Fixed Common Crossing 1:12, Journal of Failure Analysis and Prevention 19 (2019) pp. 1077–1092
doi: *https://doi.org/10.1007/s11668-019-00696-w*

[29] M. P. Sysyn, V. V. Kovalchuk, D. Jiang, Performance study of the inertial monitoring method for railway turnouts, International Journal of Rail Transportation 7 (2) (2019) pp. 103–116
doi: *https://doi.org/10.1080/23248378.2018.1514282*

[30] M. Sysyn, O. Nabochenko et al., Common crossing condition monitoring with on-board inertial measurements, Acta Polytechnica 59 (4) (2019) pp. 423–434
doi: *https://doi.org/10.14311/AP.2019.59.0423*

[31] M. Sysyn, L. Izvolt et al., Multifractal Analysis of the Common Crossing Track-Side Measurements, Civil and Environmental Engineering 15 (2) (2019) pp. 101–114
doi: *https://doi.org/10.2478/cee-2019-0014*

[32] D. M. Kurhan (2016) The basis of mathematical description for wave model of stresses propagation in railway track, Nauka ta Progres Transportu 65 (5) (2016) pp. 101–113, in Ukranian
doi: *https://doi.org/10.15802/stp2016/84032*

[33] M. B. Kurhan, D. M. Kurhan et al., Investigation of the influence of the state of the railway track in terms of softness and safety of trains, Journal Electromagnetic Compatibility and Safety on Railway Transport 14 (2017)

pp. 94–101, in Ukranian
doi: *https://doi.org/10.15802/ecsrt2017/137797*

[34] D. Kurhan, M. Kurhan, Modeling the Dynamic Response of Railway Track,
IOP Conference Series Materials Science and Engineering 708
(2019) 012013.
doi: *https://doi.org/10.1088/1757-899X/708/1/012013*

[35] M. B. Kurhan M. B., Kurhan D. M., et al., Features of stress-strain state of the
dual railway gauge, Nauka ta Progres Transportu 79 (1) (2019) pp. 51–63, in
Ukranian
doi: *https://doi.org/10.15802/stp2019/158471*

[36] M. B. Kurhan, D. M. Kurhan, Railway track representation in mathematical
model of vehicles movement, Nauka ta Progres Transportu 72 (6) (2017) pp.
40–48
doi: *https://doi.org/10.15802/stp2017/118380*

[37] A. Németh, Sz. Fischer, Glued insulated rail joints with polymer-composite
fishplates (Part 1) – Laboratory tests, Sínek Világa 58 (6) (2016) pp. 2–6, in
Hungarian

[38] A. Németh, Sz. Fischer, Investigation of glued insulated rail joints with
special fiber-glass reinforced synthetic fishplates using in continuously
welded tracks, Pollack Periodica 13 (2) (2018) pp. 77–86.
doi: *https://doi.org/ 10.1556/606.2018.13.2.8*

[39] A. Németh, Sz. Fischer, Laboratory test results of glued insulated rail joints
assembled with traditional steel and fibre-glass reinforced resin-bonded
fishplates, Nauka ta Progress Transportu 81 (3) (2019) pp. 65–86.
doi: *https://doi.org/10.15802/stp2019/171781*

[40] A. Németh, Sz. Fischer, Field tests of glued insulated rail joints with
polymer-composite and steel fishplates, in: B. Horváth, G. Horváth, B. Gaál
(Eds.), Technika és technológia a fenntartható közlekedés szolgálatában :
Közlekedéstudományi Konferencia, Universitas-Győr Nonprofit Kft., Győr,
2018, pp. 97–105.

[41] A. Németh, Sz. Fischer, Polymer composite fishplated glued insulated rail joints (part 2) – Railway track examination, Sínek Világa 60 (6) (2018) pp. 12–17, in Hungarian

[42] A. Németh, Sz. Fischer, Field tests of glued insulated rail joints with usage of special plastic and steel fishplates, Nauka ta Progress Transportu 80 (2) (2019) pp. 60–76.
doi: *https://doi.org/10.15802/stp2019/165874*

[43] Axis VM 13 (2016) [cited 2020-02-11] in Hungarian
URL
http://ftp2.myaxisvm.com/downloads.axisvm/manual/axisvm_m anual13_hu.pdf

[44] Cs. Ágh, Comparative Analysis of Axlebox Accelerations in Correlation with Track Geometry Irregularities, Acta Technica Jaurinensis 12 (2) (2019) pp. 161–177.
doi: *https://doi.org/10.14513/actatechjaur.v12.n2.501*